Physics – Uspekhi **56** (11) 1047 – 1073 (2013)

REVIEWS OF TOPICAL PROBLEMS PACS numbers: 61.46.Np, 61.48.De, **77.22. – d**, 85.35.Kt

Electronic properties of pristine and modified single-walled carbon nanotubes

M V Kharlamova

DOI: 10.3367/UFNe.0183.201311a.1145

Contents

Abstract. The current status of research on the electronic properties of filled single-walled carbon nanotubes (SWCNTs) is reviewed. SWCNT atomic structure and electronic properties are described, and their correlation is discussed. Methods for modifying the electronic properties of SWCNTs are considered. SWCNT filling materials are systematized. Experimental and theoretical data on the electronic properties of filled SWCNTs are analyzed. Possible application areas for filled SWCNTs are explored.

1. Introduction

Carbon, the sixth element in Mendeleev's Periodic Table, has a few allotropic modifications. Some have been known for a long time (diamond, graphite, amorphous carbon), while others (fullerenes, carbon nanotubes, graphene) have only recently been discovered. Tubular carbon forms were first mentioned in the C Chambers patent dated 1889 [1]. T Edison was the first to use carbon fibers in his light bulb model of 1892 [2]. In 1952, the Soviet scientists L V Radushkevich and V M Luk'yanovich synthesized hollow carbon fibers 100 nm in diameter by means of thermal decomposition of carbon monoxide on an iron catalyst [3]. The group of Japanese researchers leaded by A Oberlin synthesized in 1976 carbon fibers less than 10 nm in diameter by thermal decomposition of benzene [4, 5].

The structure of hollow carbon tubes referred to as multiwalled carbon nanotubes (MWCNTs) was comprehensively described by S Iijima in his article published in *Nature* in 1991 and devoted to the synthesis of a new allotropic modification of carbon by the arc-discharge method. That is why the discovery of MWCNTs is dated 1991. The Soviet researchers Z Ya Kosakovskaya, L A Chernozatonskii, and E A Fedorov also managed to synthesize MWCNTs in 1992 [7]. Two years later the discovery of MWCNTs (i.e., in 1993), the research teams headed by S Iijima and D Bethune independently synthesized single-walled carbon nanotubes (SWCNTs) by the arc-discharge method with the use of a metal catalyst [8, 9].

Discovered 20 years ago, the SWCNTs attracted the attention of specialists all over the world, and the properties of this new allotropic modification of carbon became the subject of extensive research. Moreover, studies of the physical properties of pristine and modified SWCNTs were most popular among the scientific community throughout the 1990s–2000s till the discovery of graphene, another allotropic modification of carbon with sp^2-hybridized carbon atoms. The SWCNT research boom was due to the great interest in the unique physical, chemical, and mechanical properties of these materials demonstrated by both the basic and applied sciences. The small diameter (less than 2 nm) and unique physical characteristics (high electrical conductivity and current density, etc.) of SWCNTs made them promising candidates for employment as elements of future nanoelectronic devices.

M V Kharlamova Department of Chemistry,
Lomonosov Moscow State University,
Leninskie gory, 119991 Moscow, Russian Federation
Tel. +7 (495) 939 59 31. Fax +7 (495) 939 09 98
E-mail: mv.kharlamova@gmail.com

Received 9 February 2013, revised 5 April 2013
Uspekhi Fizicheskikh Nauk **183** (11) 1145 – 1174 (2013)
DOI: 10.3367/UFNr.0183.201311a.1145
Translated by Yu V Morozov; edited by A Radzig

Very soon after the discovery of carbon nanotubes, the first publications on filling their internal channels appeared. Four papers published in 1993 described the encapsulation of metals and chemical compounds (lead [10], yttrium carbide [11], lead and bismuth oxides [12], and nickel [13]) into MWCNT internal channels. MWCNTs have channels of a larger diameter (on average, 5–50 nm) than SWCNTs (1–2 nm); therefore, filling internal channels of SWCNTs encountered greater difficulties that were overcome only 5 years after their discovery. In 1998, B W Smith and co-workers [14] described the synthesis of SWCNTs filled with fullerene C_{60} molecules. Another paper published in the same year by J Sloan et al. [15] reported the incorporation of $RuCl_3$ molecules into the internal channels of SWCNTs. Since then, many researchers have shown interest in filling SWCNT channels with a variety of chemical compounds.

At the beginning (the 1990s), the researchers tried to understand what substances can be introduced into SWCNT channels. In the studies published at that time, filled nanotubes were studied by high-resolution transmission electron microscopy. They showed the possibility of inserting certain compounds into the channels of single-walled nanotubes applying a special filling technique. The effectiveness of various methods and their applicability to the introduction of different substances were evaluated.

At the second stage (the 2000s) of investigations devoted to SWCNT channel filling, the researchers tried to elucidate the structure of the chemical compounds intercalated into SWCNT channels. At that time, the behavior of the inserted substances under an electron beam was studied with reference to the processes of dimerization, coalescence, and diffusion of fullerene molecules in SWCNT channels; also, attention was given to crystal clusterization and cluster rotation under these conditions. The structure of one-dimensional crystals inserted into SWCNT internal channels was considered, one- and three-dimensional structures were compared, and crystal lattice distortions were evaluated. The diameter of SWCNTs was shown to influence the structure of the developing one-dimensional crystals.

At the third stage (from 2007 till now), researchers have been trying to find out how the introduced substances influence the electronic properties of SWCNTs. The application of various research methods, such as Raman spectroscopy (RS), X-ray photoelectron spectroscopy (XPS), optical absorption spectroscopy (OAS), X-ray emission spectroscopy (XES), X-ray absorption spectroscopy (XAS), UV photoelectron spectroscopy (UPS), and photoluminescence spectroscopy (PLS), made it possible to precisely study at both the qualitative and quantitative levels modification of SWCNT electronic properties by utilizing the filling of different materials.

The objective of the present review is to analyze, systematize, and summarize the currently available literature data on the electronic properties of filled SWCNTs.

The layout of the review is as follows. Section 2 contains a description of SWCNT atomic structure. The band structure and electronic properties of SWCNTs and their relationship with the nanotube structure are considered in Section 3. Section 4 deals with a variety of methods addressing modification of SWCNT electronic properties. Section 5 summarizes and organizes into a system the available data on the electronic properties of filled SWCNTs, which were obtained in experimental and theoretical studies. Finally, possible applications of filled SWCNTs are explored in Section 6

2. SWCNT atomic structure

The structure of an ideal SWCNT can be described as a hollow cylinder having the lateral surface formed by a folded graphene sheet (hexagonal layer of carbon atoms). Each carbon atom is covalently bound to three nearest-neighbor carbons, and the angle between these bonds is 120°. The end of the SWCNT is usually capped with a fullerene hemisphere containing pentagonal carbon rings, besides hexagonal fragments. Therefore, the minimal SWCNT diameter is determined by the size of the smallest stable C_{60} fullerene, and the maximum one reaches 3 nm [16, 17]. The ratio between the length and diameter of nanotubes being 10^4 – 10^5, they belong to the class of one-dimensional nanostructures [17]. It should be mentioned that the carbon nanotubes form bundles containing hundreds of hexagonally packed SWCNTs [16–19] bound by van der Waals forces; the distance between adjacent nanotubes ranges 0.315–0.320 nm [19].

The SWCNT structure is described in terms of chiral vector ($\mathbf{C}_h$) along which a graphene sheet rolls. This vector connects two crystallographically equivalent points of the hexagonal layer of carbon atoms [the origin of coordinates and the point with coordinates (n, m), referred to as chirality indices]; therefore, the chiral vector magnitude is equal to the length of the SWCNT circumference. The chiral vector $\mathbf{C}_h$ determines the nanotube geometric structure (n, m) and is characterized by the chiral angle θ between its direction and the direction in which the adjacent hexagons have a common side.

The chiral angle varies within $0 \leqslant \theta \leqslant 30^\circ$ due to the hexagonal symmetry of the graphene layer. It determines the position of carbon hexagons inside the graphene layer with respect to the nanotube axis. For this reason, nanotubes with chirality $(n, 0)$, for which $\theta = 0^\circ$, are called zigzag carbon nanotubes. In such nanotubes, carbon–carbon bonds are parallel to the SWCNT axis. Nanotubes with chirality (n, n), for which $n = 30^\circ$, are called armchair nanotubes; C–C bonds in such nanotubes are perpendicular to the axis. All the remaining (n, m) nanotubes, for which $0 < \theta < 30^\circ$, belong to the class of chiral nanotubes [17].

3. Band structure and electronic properties of SWCNTs

Since SWCNTs are shaped like a graphene sheet rolled into a cylinder, their electronic structure is usually described in terms of graphene band structure [17]. Figure 1a shows a graphene unit cell that contains two sp^2-hybridized carbon atoms, each having four valence electrons, three of which form strong covalent σ-bonds with the three nearest neighbors, whereas nonhybridized carbon p_z-orbitals form weaker delocalized π-bonds directed perpendicular to the plane of the graphene sheet [17, 18, 20].

The energy levels related to σ-bonds are located far from the Fermi level. Due to this, they do not influence the electronic properties of graphene, whereas the bonding and antibonding π-bands of graphene intersect the Fermi level [18]. The first Brillouin zone of graphene has the form of a hexagon with three high-symmetry points Γ, K, and M (Fig. 1b) [17]. Nonhybridized p_z-orbitals of carbon give rise

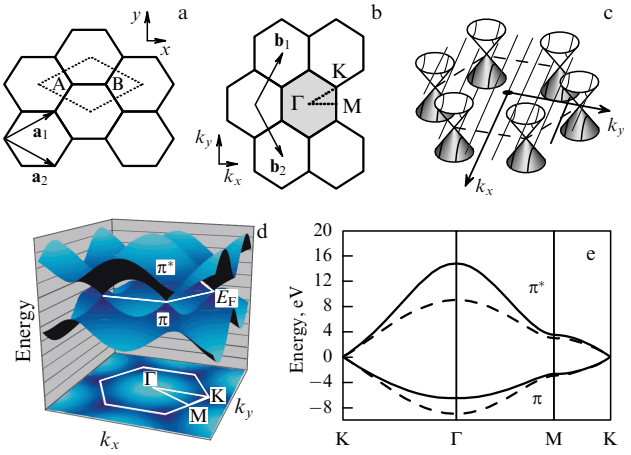

Figure 1. (Color online.) Graphene unit cell (marked by a dotted line) (a) and first Brillouin zone (grey color) (b) [17]; (c) schematic of intersection of cone-shaped graphene conduction and valence bands in six corners of the first Brillouin zone (K points) at the Fermi level [21]; (d) energy diagram of graphene sheet in the first Brillouin zone; (e) section of graphene energy diagram along the perimeter of ΓMK triangle; the diagram was constructed using the following parameters: $\gamma_0 = 3.033$ eV, $\varepsilon_{2p} = 0$, and $s = 0.129$ (asymmetric dispersion — solid line) or $s = 0$ (symmetric dispersion — dashed line) [23, 24].

to conduction and valence bands in the form of cones near the Fermi level (Fig. 1c) [21, 22]. The band structure of graphene is unique in that the bottom of the conduction band touches the top of the valence band at the Fermi level in the six corners (points K) of the first Brillouin zone; hence, the semimetallic properties of graphene [21, 22].

In accordance with the tight-binding model, the formula for energy dispersion of π-bands of the graphene sheet can be represented in the form [17, 24]

$$E^{\pm}_{g2D}(\mathbf{k}) = \frac{\varepsilon_{2p} \pm \gamma_0 \omega(\mathbf{k})}{1 \mp s\omega(\mathbf{k})}\,, \tag{1}$$

where γ_0 is the transfer integral ($\gamma_0 > 0$), ε_{2p} is the energy of the 2p-atomic orbital position, and s is the overlap integral of the electron wave functions of neighbor positions. The '+' and '−' signs in the numerator and denominator refer to the antibonding π* energy band and the bonding π band of graphene, respectively.

Function $\omega(\mathbf{k})$ can be written out in the following form [17, 24]

$$\omega(\mathbf{k}) = \sqrt{1+4\cos\left(\frac{\sqrt{3}k_x a}{2}\right)\cos\left(\frac{k_y a}{2}\right)+4\cos^2\left(\frac{k_y a}{2}\right)}\,, \tag{2}$$

where a is the lattice parameter of the hexagonal carbon layer, and $a = \sqrt{3}\,a_{c\text{–}c} \approx 0.246$ nm ($a_{c\text{–}c}$ is the length of the C–C bond, equal to 0.142 nm).

Figure 1d illustrates the schematic energy diagram of a graphene sheet in the first Brillouin zone. Figure 1e shows the diagram section along the perimeter of the ΓMK triangle; the diagram was constructed using the following parameters: $\gamma_0 = 3.033$ eV, $\varepsilon_{2p} = 0$, and $s = 0.129$ (asymmetric dispersion — solid line) or $s = 0$ (symmetric dispersion — dashed line). The upper and lower curves in the diagram correspond to the antibonding π* energy band and the bonding π band of the graphene, respectively. These curves intersect at points K at the Fermi level [23, 24].

When the overlap integral is zero, it follows from Eqn (1) that π* and π bands become symmetric near $E = \varepsilon_{2p}$. Using this approximation, the energy dispersion function of the graphene sheet π bands takes the form [24, 25]

$$E^{\pm}_{g2D}(k_x, k_y) = \pm\gamma_0\sqrt{1+4\cos\left(\frac{\sqrt{3}\,k_x a}{2}\right)\cos\left(\frac{k_y a}{2}\right)+4\cos^2\left(\frac{k_y a}{2}\right)}\,. \tag{3}$$

Because SWCNTs are shaped like a graphene sheet rolled into a cylinder, the boundary conditions imposed on the structure of these objects are different: unlike graphene, carbon nanotubes can be regarded as infinitely extended only in the direction of their axes. Therefore, the wave vector having the same direction as the translation vector **T** changes continuously (in the case of an infinitely long SWCNT), whereas the wave vector, the direction of which coincides with that of the chiral vector $\mathbf{C}_h$, has a set of discrete components [17]. Due to this, energy dispersion in the one-dimensional case can be defined as [17, 24]

$$E^{\pm}_{1D}(k) = E^{\pm}_{g2D}\left(k\,\frac{\mathbf{K}_2}{|\mathbf{K}_2|} + \mu\,\mathbf{K}_1\right), \tag{4}$$

where k is the one-dimensional wave vector directed along the SWCNT axis ($-\pi/T < k < \pi/T$ and $\mu = 1 \ldots N$), $\mathbf{b}_1$ and $\mathbf{b}_2$ are the vectors of the graphene sheet reciprocal lattice,

$$\mathbf{K}_1 = 2\,\frac{(2n+m)\,\mathbf{b}_1 + (2m+n)\,\mathbf{b}_2}{N_C N_R}\,, \quad \mathbf{K}_2 = 2\,\frac{(m\mathbf{b}_1 - n\mathbf{b}_2)}{N_C}\,,$$

N_C is the number of carbon atoms in a unit cell of the SWCNT, $N_C = [4(n^2 + nm + m^2)/N_R]$, and N_R is the greatest common divisor of numbers $(2m + n)$ and $(2n + m)$.

In the case of armchair (n, n) nanotubes, the application of periodic boundary conditions to derive energy dispersion formulas yields a small number of allowed wave vectors $k_{x,q}$ having the same direction as the chiral vector $\mathbf{C}_h$ and satisfying the following expression [17]:

$$n\sqrt{3}\,k_{x,q}a = 2\pi q\,, \quad (q = 1 \ldots 2n)\,. \tag{5}$$

Figure 2 shows schematically parts of a unit cell (a) and the first Brillouin zone (b) of an armchair nanotube (n, n).

Substitution of the respective expression for $k_{x,q}$ into (3) gives the wave vector dependence of energy for armchair nanotubes (n, n) [17]:

$$E^{\text{armchair}}_q(k) = \pm\gamma_0\sqrt{1+4\cos\left(\frac{q\pi}{n}\right)\cos\left(\frac{ka}{2}\right)+4\cos^2\left(\frac{ka}{2}\right)}, \tag{6}$$

where $-\pi < ka < \pi$ and $q = 1 \ldots 2n$, while vector k is parallel to vector $\mathbf{K}_2 = (\mathbf{b}_1 - \mathbf{b}_2)/2$.

At point $k = 2\pi/3a$, the dispersion formula assumes the following form

$$E^{\text{armchair}}_q\left(k = \frac{2\pi}{3a}\right) = \pm\gamma_0\sqrt{2+2\cos\left(\frac{q\pi}{n}\right)}\,. \tag{7}$$

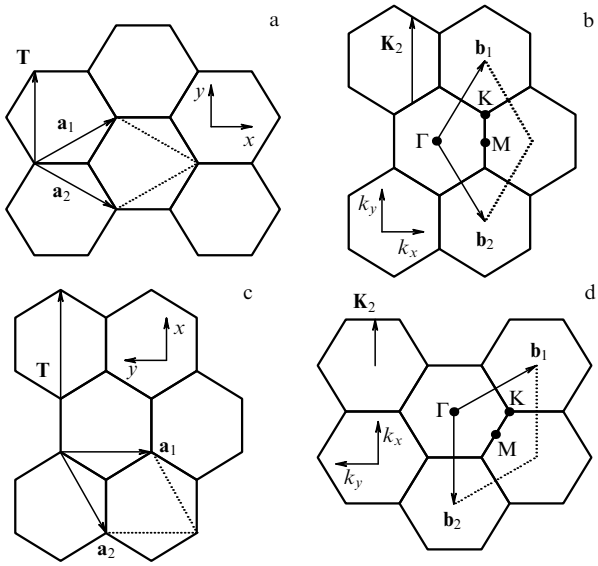

Figure 2. Part of a unit cell and the first Brillouin zone of an armchair (n, n) nanotube (a, b) and zigzag $(n, 0)$ nanotube (c, d) [17].

It follows from expression (7) that energy bands undergo degeneracy at point $k = 2\pi/3a$, given $q = n$ regardless of the value of n. It means that all armchair (n, n) nanotubes possess metal type conduction.

The formulas for energy dispersion in zigzag nanotubes are derived by imposing periodic boundary conditions on the wave vector k_y [17]:

$$nk_{y,q}a = 2\pi q \quad (q = 1 \ldots 2n)\,. \tag{8}$$

Figure 2 depicts schematically parts of a unit cell (c) and the first Brillouin zone (d) of a zigzag $(n, 0)$ SWCNT.

Substitution of the respective expression for $k_{y,q}$ into formula (3) gives [17]

$$E_q^{\text{zigzag}}(k) = \pm\gamma_0\sqrt{1 + 4\cos\left(\frac{\sqrt{3}\,ka}{2}\right)\cos\left(\frac{q\pi}{n}\right) + 4\cos^2\left(\frac{q\pi}{n}\right)}, \tag{9}$$

where $-\pi/\sqrt{3} < ka < \pi/\sqrt{3}$, and $q = 1 \ldots 2n$.

In the center of the Brillouin zone ($k = 0$), the dispersion formula assumes the form

$$E_q^{\text{zigzag}}(k = 0) = \pm\gamma_0\left(1 + 2\cos\left(\frac{q\pi}{n}\right)\right). \tag{10}$$

It follows from expression (10) that valence and conduction bands intersect at $q = 2n/3$, which accounts for metal type conductivity of zigzag $(n, 0)$ nanotubes at $n = 3l$ (where l is an integer) and semiconducting type conductivity for $n \neq 3l$. The calculated results are confirmed by experimental data [26].

Figure 3 presents a map of the distribution of metallic and semiconducting nanotubes depending on the chiral vector $\mathbf{C}_h$ [22]. On the whole, nanotubes with arbitrary values of indices n and m show metallic properties at $n - m = 3l$ (l is an integer) and semiconducting properties at $n - m = 3l \pm 1$ [18, 27, 28]. In a sample of SWCNTs not separated by conductivity type, one third of the nanotubes had metallic properties and the remaining two thirds show semiconducting properties [28].

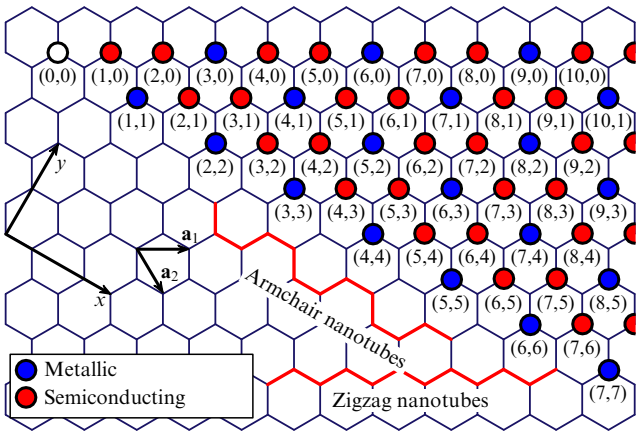

Figure 3. (Color online.) Map of the distribution of metallic and semiconducting nanotubes depending on the chiral vector $\mathbf{C}_h$ [22].

The density of SWCNT electron states deduced from Eqn (4) is expressed as [24]

$$D(E) = \frac{T}{\pi N_C}\sum_{\pm}\sum_{v=1}^{N}\int\left|\frac{\mathrm{d}E_{1D}^{\pm}(k)}{\mathrm{d}k}\right|^{-1}\delta\left(E_{1D}^{\pm}(k) - E\right)\mathrm{d}E\,, \tag{11}$$

where summation is performed over the number (N) of one-dimensional conduction (+) and valence (−) bands. In the case of metallic nanotubes, the density of electron states is constant at the energy equaling the Fermi energy and is inversely proportional to nanotube diameter d_t [24]:

$$D(E_F) = \frac{a}{2\pi^2\gamma_0 d_t}\,. \tag{12}$$

It is worthy of note that van Hove singularity is an important feature of the density of SWCNT electron states. When the energy dispersion function passes through local maxima and minima, the denominator in expression (11) becomes equal to unity, which results in an abrupt jump in the density of electron states. This situation is illustrated by Fig. 4 showing the band structures of armchair (5, 5) (a), zigzag (9, 0) (b) and (10, 0) (c), and chiral (8, 2) (d) nanotubes, and the respective densities of electron states [18]. It follows from Fig. 4 that (5, 5), (9, 0), and (8, 2) nanotubes ($n - m = 3l$) have a nonzero density of electron states near the Fermi level. For this reason, they are characterized by metallic conductivity, whereas (10, 0) SWCNTs ($n - m = 3l \pm 1$) possess zero conductivity and, therefore, exhibit semiconducting properties.

The presence of van Hove singularities is an important feature of SWCNTs, which was observed in studies of nanotube properties by scanning tunneling spectroscopy (STS) [29–32], optical absorption spectroscopy [33–35], and Raman spectroscopy [36–40].

The energies of electronic transitions between the respective van Hove singularities of the valence and conduction bands are related to the SWCNT diameter d_t by the expression [41]

$$\Delta E_{ii} = \frac{2k\gamma_0 a_0}{d_t}\,, \tag{13}$$

where k is an integer, and a_0 is the distance between neighboring carbons (~ 0.14 nm). This means that electronic transition energies are inversely proportional to the

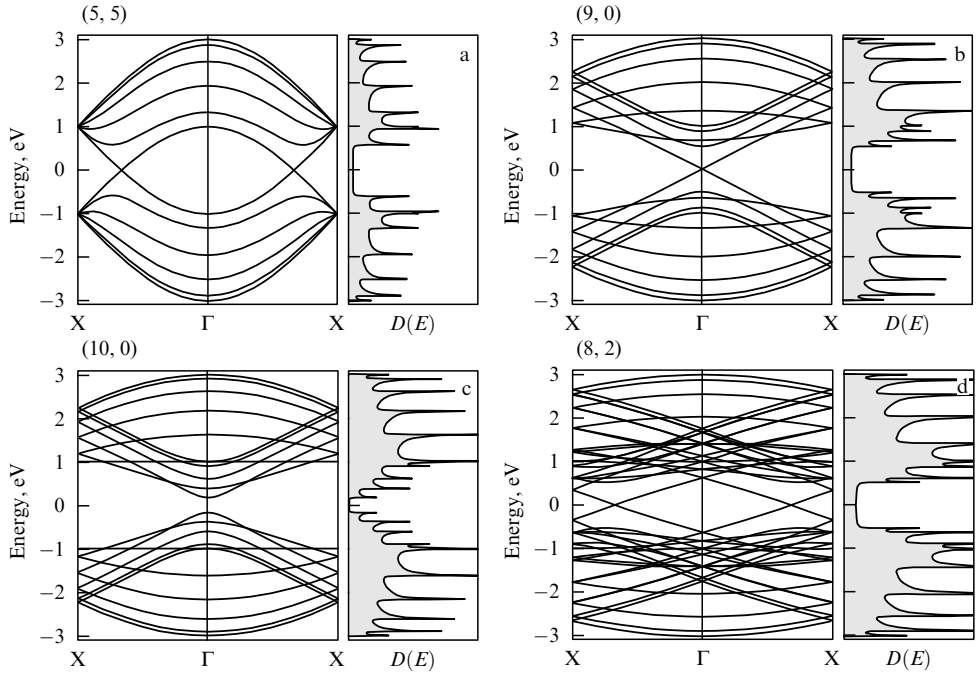

Figure 4. Band structures and respective densities of electron states for armchair (5, 5) (a), zigzag (9, 0) (b) and (10, 0) (c), and chiral (8, 2) (d) SWCNTs [18].

SWCNT diameter. Calculations suggest at least four electronic transitions ($k = 1$, 2, 4, 8) in semiconducting nanotubes, and two transitions ($k = 3$, 6) in metallic ones [42, 43]. The theoretical dependences of electronic transition energies between van Hove singularities on SWCNT diameter, known as the Kataura plot, are widely used to determine SWCNT diameter and chirality from optical measurements [44].

Thus far, we have considered the SWCNT electronic structure in terms of the band structure of a graphene sheet with the use of periodic boundary conditions imposed on the wave vector of the same direction as the chiral vector $\mathbf{C}_h$. In this model case, we neglected curvature effects in the graphene sheet disregarding the fact that the lengths of C–C bonds parallel and perpendicular to the SWCNT axis are somewhat different. In such a case, the basis vectors of the hexagonal layer of carbon atoms have different magnitudes, and the p_z-orbitals of carbons are not strictly parallel to the SWCNT axis. Moreover, the binding of carbon atoms was considered regardless of the contribution from sp^3-hybridization of the orbitals likely to arise from the intersection of π and σ bands [18].

But it turned out that taking into account these effects in the calculation of the SWCNT band structure results in only armchair (n, n) nanotubes possessing metallic properties. Nanotubes for which $n - m = 3l$ (l is an integer) are low bandgap semiconductors, whereas all other SWCNTs are their wide bandgap counterparts [18]. The width of the so-called secondary band gap (arising from the curvature of the graphene layer) in low bandgap semiconducting nanotubes is inversely proportional to the diameter squared [18, 45]. For example, this dependence for quasimetallic zigzag SWCNTs ($\theta = 0°$) has the form [18]

$$\Delta E_g^2 = \frac{3\gamma_0 a_0^2}{4d_t^2} \,. \qquad (14)$$

However, this quantity is so small that it can be assumed for practical purposes that nanotubes with $n - m = 3l$ possess metallic properties at room temperature [18].

In previous paragraphs, we have considered the band structure of individual single-walled carbon nanotubes, but synthesized SWCNTs are usually packed into bundles composed of 10–100 nanotubes of different diameters and chiralities, and even the ideal packaging of identical nanotubes may result in a change in their electronic structure. For example, it was shown by the first-principle calculations that the breaking of mirror symmetry of armchair (10, 10) nanotubes due to their interaction within a bundle leads to the formation of a pseudo-bandgap as wide as 0.1 eV [18, 46] (Fig. 5). This was also confirmed experimentally by low-temperature scanning tunneling microscopy (STM) [47]. Simultaneously, it was shown that metal-type conductivity is inherent in both armchair (6, 6) SWCNTs packed in a hexagonal bundle and isolated (6, 6) SWCNTs [48, 49].

Thus, taking account of the curvature effects of the graphene sheet and of the nanotube interaction within the

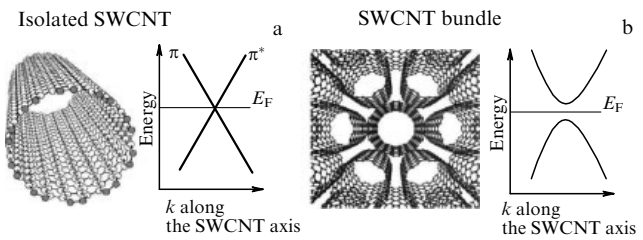

Figure 5. (a) Schematic intersection of two linear bands (bonding π band and antibonding π^* band) for an isolated (n, n) SWCNT, and (b) schematic of repulsion between bands in a nanotube bundle resulting from the breaking of mirror symmetry [18].

bundle in calculations of SWCNT band structure may substantially change their results.

Moreover, we have so far considered the band structure of defectless nanotubes, whereas in reality the walls of SWCNTs may contain defects, such as the most widespread five- and seven-membered carbon cycles responsible for a change in the chiral vector and electronic structure [18, 50, 51]. It should be emphasized that the directional introduction of defects into SWCNT walls is a promising tool for the modification of their electronic properties, opening up new possibilities for the further application of nanotubes in nanoelectronic devices [18, 52]. Because SWCNTs have either metallic or semiconducting conductivity, depending on their structure, the directional introduction of a pair of defects (five-membered plus seven-membered carbon cycles) may cause metal–semiconductor, semiconductor–semiconductor or metal–metal junctions as have been confirmed both theoretically [53–57] and experimentally [58, 59].

4. Methods for modifying the electronic properties of SWCNTs

There are a few approaches to the modification of SWCNT electronic properties (Fig. 6). They include:

(1) chemical modification of the outer surface of nanotubes with the use of functional groups;

(2) modification of the outer surface of SWCNTs with the use of molecules forming no chemical bonds;

(3) substitution of carbon atoms in the walls of nanotubes by other atoms;

(4) intercalation of nanotube bundles;

(5) electrochemical doping;

(6) filling of SWCNT internal channels.

Each of these approaches represents a separate line of SWCNT inquiry with its own history, characteristic features, and advantages and disadvantages, depending by and large on the concrete research goal. Each method is highly specific in terms of both the process design and the properties of the resulting materials, developing independently of other methods without competing with them and likely finding concrete applications in the future. It is therefore incorrect to compare the advantages and disadvantages of these methods. In view of this, only a brief description of each method is presented below.

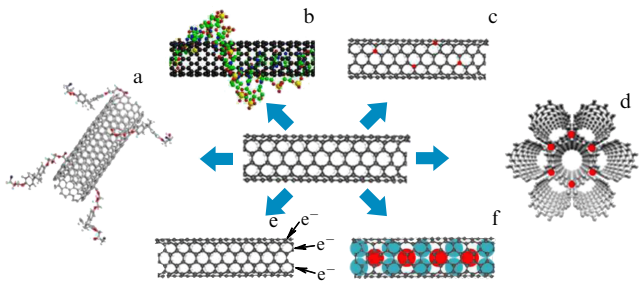

Figure 6. (Color online.) Methods for modification of SWCNT electronic properties: (a) chemical modification of the outer surface of nanotubes with the use of functional groups; (b) modification of the outer surface of SWCNTs with the use of molecules forming no chemical bonds; (c) substitution of carbon atoms in the walls of nanotubes by other atoms; (d) intercalation of nanotube bundles; (e) electrochemical doping, and (f) filling of internal channels of SWCNTs.

4.1 Chemical modification of the outer surface of SWCNTs with the use of functional groups

Chemical modification of the outer surface of an SWCNT implies the attachment (usually by covalent bonding) of various functional groups to it [60]. The advent of this method was due to the necessity of dissolving and dispersing nanotubes, because pristine SWCNTs are insoluble in all known organic solvents and aqueous solutions [60, 61]. Nanotubes can be dispersed ultrasonically, but they rapidly precipitate after the process is completed [60]. Also, SWCNTs can interact with various compounds [16, 62–85]. The possibility of forming nanotube-based supramolecular complexes opens up new prospects for their application in nanodevices. Nanotubes can enter into chemical reactions that enhance their solubility, which allows them to be introduced into inorganic, organic, and biological systems [60]. Moreover, the attachment of functional groups to the walls of SWCNTs may change their electronic properties [61].

The methods devised for chemical modification of the outer surface of SWCNTs can be classified based on the type of the functional groups to be attached to it. *Fluorination* of nanotubes with elemental fluorine at 25–600 °C [86–92] leads to the attachment of fluorine to carbon atoms, which causes their transition to the sp^3-hybridized state, accompanied by reorganization of the band structure of both metallic and semiconducting nanotubes; this process yields materials with a wide bandgap [60]. Extensive studies of the nanotube fluorination process are underway using transmission electron microscopy [88], scanning tunneling microscopy [93], X-ray photoelectron spectroscopy [94–98], X-ray absorption spectroscopy [95, 99], and theoretical calculations [100–107]. Results of elemental analysis indicate that maximum fluorination of nanotubes can be described by empirical formula C_2F [60]. Notice that the fluorine atoms can be removed from the surface of nanotubes by treating it with a hydrazine solution in propanol-2 [87, 88, 91] followed by thermal treatment [108, 109].

It was demonstrated in Ref. [110] that SWCNT *iodination* resulting in covalent attachment of iodine to the outer surface of SWCNTs does not change their electronic properties.

Simultaneously, it was shown that the *cycloadditions of organic molecules* to the SWCNT surface may cause a charge transfer between functional groups and the nanotube walls [60, 111–116]. By way of example, Ref. [113] describes a method for the attachment of dichlorocarbene to SWCNT walls, with 2% of the carbon atoms being covalently bound to these groups. This resulted in a marked change in the electronic properties of metallic SWCNTs.

Charge transfer between the SWCNT wall and a functional group was also observed in the products of *diazonium salt radical addition* [117–123]. Furthermore, methods for the selective attachment of water-soluble diazonium salts to metallic nanotubes have been developed [118, 122, 123].

4.2 Modification of the outer surface of SWCNTs with the use of molecules forming no chemical bonds

Modification of the outer surface of SWCNTs is possible not only by means of covalent attachment of functional groups but also by wrapping nanotubes with a variety of molecules, e.g., polymers [62, 85], polycyclic aromatic compounds [124–128], surfactants [129–131], and biological molecules [76], or by adsorption of molecules on SWCNT walls without the formation of chemical bonds. The interaction between molecules and nanotubes is mediated through van der Waals

forces and $\pi-\pi$ stacking (i.e., noncovalent interaction between molecules containing aromatic rings due to intermolecular overlap between p-orbitals in π-conjugate systems) [60]. The choice of a concrete method to modify the SWCNT outer surface depends on a specific research goal; however, it does not necessarily result in a change in the nanotube electronic properties, which is sometimes regarded as an advantage [60].

Modification of the electronic properties of nanotubes may be effected by their treatment with solvents and dispersers [60, 132]. Thus, it was shown that even the use of such conventional dispersers as sodium dodecyl sulfate (SDS) and polythiophene may lead to a change in the SWCNT electronic structure [133, 134]. Reference [135] reported the influence of aromatic and aliphatic solvents containing electron donor and electron acceptor groups on nanotube electronic properties. It was revealed that when molecules of the solvents are adsorbed at the outer surface of SWCNTs, a charge transfer accompanied by a shift of the Fermi level of SWCNTs occur between these molecules and the tube walls. In this way, the nanotubes can be doped. The use of aniline and butylamine, the molecules of which contain the $-NH_2$ group, results in donor doping of SWCNTs, while the use of nitrobenzene and nitromethane containing the $-NO_2$ group leads to acceptor doping, whereas neither benzene nor hexane affects the electronic properties of nanotubes.

The influence of gases adsorbed at the surface of SWCNTs on their electronic properties was evaluated in Refs [136, 137]. The studies revealed a dramatic difference between electric conductivity, thermoelectromotive force, and local density of electron states measured in the air and a vacuum [136]. Moreover, these parameters changed reversibly upon insignificant changes in adsorbed gas concentrations; even the transition of semiconducting SWCNTs to metallic state could be observed [136]. The authors of Ref. [137] documented both the increase and decrease in measured electrical resistivity of SWCNTs placed in an atmosphere of NO_2 or NH_3, when compared with the same parameters in a vacuum. The data obtained gave reason for a conclusion about the possibility of using SWCNTs as gas sensors [136, 137].

4.3 Substitution of carbon atoms in the walls of SWCNTs by other atoms

Obviously, a direct consequence of the substitution of carbon atoms in the walls of SWCNTs by other atoms is the modification of their electronic properties [61]. In this case, the SWCNT electronic structure will depend on the type and concentration of the doping atoms rather than the nanotube structure [138]. Therefore, this method makes possible the intentional modification of SWCNT electronic properties. Moreover, the substitution of carbon atoms can enhance the oxidation resistance of SWCNTs and their reactivity in chemical processes involving doping atoms [61].

The first work [139] concerning the modification of nanotube electronic properties by substituting carbon atoms dates to 1993, i.e., immediately after the discovery of SWCNTs [8, 9]. Since then, numerous studies on the synthesis and investigations of SWCNTs doped with nitrogen [140–150] and boron [147, 151–158] have been published.

Evidently, the method under consideration allows two parameters to be varied: the type and concentration of the doping element. Nitrogen and boron are carbon's neighbors in the Periodic Table; therefore, the utilization of these elements, having similar chemical properties to carbon, looks like a logical choice for the substitution of carbon atoms in nanotubes. Recall that carbon has the electron configuration $1s^2 2s^2 2p^2$, nitrogen — $1s^2 2s^2 2p^3$, and boron — $1s^2 2s^2 2p^1$. This means that direct substitution of carbons by nitrogen and boron atoms must lead to donor doping and acceptor doping, respectively.

Indeed, it was theoretically predicted in Ref. [139] that boron doping (B:C = 1:80) of SWCNTs with chirality (8, 0) gives rise to the acceptor level in the SWCNT band structure, which is positioned 0.16 eV above the Fermi level. The electronic properties of boron-doped SWCNTs were later explored in Refs [147, 153, 154, 156, 158]. Simultaneously, it was shown that direct substitution of carbon atoms by nitrogens results in donor doping of nanotubes [138, 159–162].

However, this is not the only way in which nitrogen atoms can be incorporated into the hexagonal lattice of carbon atoms of SWCNT walls. The incorporation of a nitrogen atom may result in a defect formation in the SWCNT wall, which causes rearrangement of carbon atoms, after which only two of them are bound to the nitrogen atom [138, 159, 162, 163]. In such a substitution, doping levels may emerge either above or below the Fermi level, depending on the new wall structure which accounts for acceptor or donor doping of nanotubes, respectively, as demonstrated both in theory [160, 164] and experiment [144, 147, 149, 150].

As shown earlier, the second parameter varied in the method of interest is the concentration of doping elements. Indeed, the change in electronic properties of SWCNTs at low-level doping (e.g., 0.2 at.% N [140] or 0.3 at.% N [141]) can be considered in the context of the rigid band model [138, 159, 165]. However, high-level doping is associated with the formation of so-called heteronanotubes, which makes this model inapplicable [138, 159]. It should be noted that the problem of boundary concentration remains to be resolved [138].

As shown theoretically in Ref. [156] dealing with heteronanotubes having the empirical formula BC_3, high-level boron doping of nanotube walls gives rise to a 0.4-eV-wide bandgap and an additional energy level positioned 0.1 eV higher than the Fermi level. Calculations in Ref. [166] showed simultaneously that nitrogen-containing heteronanotubes having the empirical formula C_3N_4 are semiconductors with a bandgap ~ 3.0 eV in width.

Phosphorus and silicon can also substitute atoms in the walls of SWCNTs [167–169]. Simulations show that the incorporation of silicon atoms into the hexagonal lattice of carbon atoms causes distortion of the cylindrical surface of the nanotubes, which enhances their reactivity in chemical processes [167, 168].

4.4 Intercalation of nanotube bundles

Modification of the electronic properties of SWCNTs can be made by the intercalation of their bundles with simple substances (sometimes compounds) exhibiting acceptor or donor properties. This process is analogous to the intercalation of graphite and fullerenes described earlier in Refs [170] and [171], respectively. But unlike fullerenes, SWCNTs can be doped with both electron donors and acceptors.

The first two studies concerning SWCNT intercalation with potassium (electron donor) and bromine (electron acceptor) were published in 1997. They studied the resulting nanosystems by Raman spectroscopy [172] and measured

their electrical resistance [173]. Thereafter, it was shown that donor doping of nanotubes, accompanied by a rise in the Fermi energy and charge transfer from the dopants to the tube walls, is possible by the intercalation of alkali metals (Li, Na, K, Rb, Cs) and Ba into SWCNTs [71, 113, 174–200]. Acceptor doping of SWCNTs associated with a downward shift of the Fermi level and charge transfer from the walls to the doping agents can be performed by the intercalation of bromine, iodine, $FeCl_3$, $AuCl_3$, HNO_3, H_2SO_4, and HCl molecules [35, 113, 133, 174, 180, 186, 192, 201–212].

The substances being intercalated fill triangular cavities between nanotubes in a bundle, usually without the formation of chemical bonds between the inserted atoms or molecules and the nanotube walls. At the same time, Ref. [189] reported local interactions between barium and single-walled carbon nanotubes intercalated with this metal.

Usually, intercalation does not change the structural properties of isolated SWCNTs. According to X-ray and electron diffraction measurements, this process simultaneously leads to a disorder in the hexagonal packing of SWCNTs within a bundle due to a greater intertube spacing [175, 176, 180, 181, 187, 191]. The structural disorder in the bundle increases with a rise in the radius of the alkali dopant [180]. Moreover, intercalation proved to be selective with respect to the diameter of the SWCNT under doping by agents possessing both donor (K) and acceptor ($FeCl_3$) properties [213].

It was demonstrated that the maximum doping level in the intercalation of alkali metals (K, Rb, Cs) corresponds to an empirical formula MC_7 [188], which is slightly higher than the maximum potassium doping level in graphite (KC_8) [170, 214]; this is somewhat different from the level of fullerene doping (K_6C_{60}) [215]. In the case of lithium doping, the maximum metal concentration in nanotubes corresponds to empirical formulas LiC_6 [183, 190] and $Li_{1,2}C_6$ [178], depending on the method of intercalation.

It was reported that the intercalation of nitric acid into an SWCNT bundle increases the intertube spacing by 0.185 nm following treatment with a strong solution for 2 hours [201]. This process was shown to be reversible. Prolonged acid treatment of nanotubes (over 12 hours) destroyed them [201], presumably due to oxidation and the formation of defects in the nanotube walls [79, 216]. References [133, 201, 204, 206, 210, 212] described the modification of SWCNT electronic structure by treating nanotubes with strong solutions of sulfuric, nitric, and hydrochloric acids. These studies showed that intercalation results in acceptor doping of SWCNTs [204] with the formation of a doping level near the Fermi level [217] and the occurrence of charge transfer [201, 212].

It was shown in Ref. [35] that the maximum bromine doping level of SWCNTs corresponds to the empirical formula BrC_7, which it was much higher than in the case of Br_2C_{52} described in paper [173], even though the authors of the latter publication observed marked modification of the SWCNT Raman spectrum upon bromine intercalation into nanotubes; this effect was attributed to charge transfer from the nanotubes to the intercalated molecules [172].

Intercalation of melted iodine resulted in a doping level corresponding to the empirical formula IC_{12} [205] and caused disorder in the hexagonal packing of nanotubes in the bundle. Deintercalation of iodine failed to restore the initial packaging of SWCNTs [205]. It was revealed that gaseous iodine fills only triangular cavities between nanotubes in the bundle, whereas intercalation of melted iodine gave rise to spirals formed from polyiodide chains inside SWCNT channels; their orientation with respect to the SWCNT wall depended on the nanotube chiral vector [203]. The authors attributed this fact to the higher reactivity of melted iodine [203].

The electronic properties and charge transfer in SWCNTs intercalated with electron donors and acceptors were investigated by Raman spectroscopy [113, 172–174, 186, 192, 202, 205, 210, 213, 218–220], optical spectroscopy [35, 113, 183, 190, 209, 221, 222], electron energy loss spectroscopy (EELS) [177, 188, 189, 191, 198, 209, 222, 223], electron spin resonance (ESR) [181, 182, 197, 224, 225], and XPS techniques [184, 185, 194, 195, 199, 200], and by measuring the transport properties [173, 176, 178, 187, 222, 226]. It was shown that the intercalation of SWCNTs may cause a shift of up to 1.3 eV of the Fermi level [193]. To recall, intercalation is usually a reversible process, as was demonstrated by K and Cs intercalation as early as 1998 [177, 198]. However, deintercalation can be complicated by the instability of the resultant systems under certain conditions, e.g., in the air [61]. Such systems may find application in the development of energy storage devices after optimization of methods for reversible intercalation of SWCNTs [61].

4.5 Electrochemical doping

Doping of SWCNTs is possible by charging in an electrochemical cell. This process makes possible intentional modification of the nanotube electronic structure and ensures precise control of the doping level [227]. Electrochemical doping changes the position of the SWCNT Fermi level in proportion to the applied voltage [227]. As shown in paper [228], the coefficient of proportionality ranges 0.4–0.7 eV V^{-1}. The electrochemical technique makes possible SWCNT doping under conditions excluding chemical modification or damage of nanotubes by choosing a proper electrolyte, a range of voltages to be applied, the materials of the electrodes, and other experimental characteristics [227].

The first electrochemical study of SWCNTs was published in 1999 [229]. Later studies of nanotube properties under electrochemical charging were conducted with the use of voltamperometry [230–234] and spectroelectrochemical methods [210, 225, 228, 233–255]. The former technique makes possible donor and acceptor doping of SWCNTs in a single experiment, and the cyclic voltamperograms obtained permit one to assess the reversibility of these processes [227]. The spectroelectrochemical technique provides a powerful tool for the study of SWCNT electronic properties, because it combines the advantages of electrochemical and spectroscopic methods and permits comprehensively evaluating the modification of nanotube spectra, which corresponds to the changes in their electronic properties resulting from electrochemical doping [256].

The electrochemical approach is usually combined with Raman spectroscopy or optical spectroscopy in the visible and near-infrared regions. In either case, *in situ* experiments make use of a three-electrode electrochemical cell in which SWCNTs serve as the working electrode.

Raman spectra of nanotubes under electrochemical charging were first measured in 1999 [210]. The real process included electrochemical doping of nanotubes and their intercalation with sulfuric acid used as an electrolyte [227]. In 2000, the measurements were made in traditional electrolyte solutions, such as aqueous [233] and aprotonic (tetrahydrofuran) [225] solutions. Later on, many authors studied

SWCNT properties in aqueous electrolyte solutions [228, 235–241, 249–255], acetonitrile [234, 242, 243, 245, 246], and ionic fluids [244]. SWCNTs were usually used in the form of thin films deposited onto an inert metal substrate (Au, Hg, Pt) [233, 234, 236, 237, 243–245, 249–251] or in the form of buckypaper [235, 240, 252–254, 257].

The optical absorption spectra of electrochemically charged nanotubes were measured for the first time in 2000 [233]. Unlike the above Raman spectroscopy technique, optical spectroscopy technique requires that nanotubes be deposited onto an optically transparent conducting material, e.g., indium–tin oxide (ITO) [233, 234, 243, 244] or a thin semitransparent platinum film [247, 248], and it employs aqueous [233] and acetonitrile [234, 243, 247, 248] electrolyte solutions or ionic fluids [244]. The results of these measurements were shown to agree with those obtained in the studies of SWCNTs intercalated with electron donors and acceptors [35, 190, 218, 221].

Generally speaking, electrochemical doping may find a variety of applications [258–262]. In particular, electrochemical studies of nanotubes are motivated by the possibility of utilizing them for hydrogen storage [263, 264], and the construction of batteries [265–267], supercapacitors [230, 231], sensors [258, 262], and nanoelectronic devices [228, 268–270]. However, these electrochemical studies need highly sensitive equipment, much time to prepare an experimental setup, and time-consuming experimentation and data processing to be conducted [256]. Moreover, spectroscopic studies under electrochemical charging should be taken in special electrochemical cells and the choice of electrolytes, materials for electrodes, or other parameters is limited by the spectroscopy requirements, which may dictate the use of materials with electrochemically disadvantageous properties [256].

4.6 Filling internal channels of SWCNTs

This method is based on the encapsulation of simple substances and compounds of various chemical natures into the internal channels of SWCNTs. Thus far, experiments on filling internal channels of SWCNTs with more than 150 substances have been reported. Figure 7 presents their classification by chemical nature, whereas Table 1 summarizes the results of almost 100 studies published in the past 15 years and mentions concrete filling materials.

These materials include atoms, molecules, chemical elements (encapsulated as nanowires, clusters, or nanocrystals), and chemical compounds. The encapsulation of *atoms* into the channels of SWCNTs is a challenging experimental task; only a few examples are reported in the literature. One is the formation of spirals from polyiodide chains described in Refs [203, 271, 272]. Moreover, metallic caesium [273, 274] and carbon [275] were also shown to form atomic chains inside SWCNT channels.

The first *molecule* encapsulated into an SWCNT channel was the C_{60} fullerene [14]. Thereafter, many research groups reported on synthesis of similar nanostructures and filling nanotube channels with other fullerenes (C_{70}, C_{78}, C_{80}, C_{82}, C_{90} [216, 276–294]); endohedral fullerenes ($M@C_{82}$, where M = Ca, La, Ce, Sm, Gd, and Dy) [279, 284, 287, 295–302], $M_2@C_{80}$, where M = La and Ti, [303, 304], $Sc_2@C_{84}$ [305], $Gd_2@C_{92}$ [306], $M_3N@C_{80}$, where M = Sc, Dy, and Er [283, 307–309], and $N@C_{60}$ [289]; exohedral fullerenes ($C_{60}O$ [310], $C_{60}Cs$ [311]); C_{60}/Re, Os carbonyl complexes [312–314]; fullerenes modified by $C_{61}(COOH)_2$ and $C_{61}(COOC_2H_5)_2$ functional groups [283, 315]; C_{60} with alkyl chains [316]; C_{60} with an organic Cd complex [317]; metallocenes (ferrocene $(C_5H_5)_2Fe$ [318–329], cobaltocene $(C_5H_5)_2Co$, $(C_5H_4C_2H_5)_2Co$ [330], cerocene $(C_5H_5)_3Ce$ [331, 332]); and other organic molecules, such as Pt (II) [329, 333] and Co (II) [334] acetylacetonates, ortho-carborane [335], Zn (II) and Pt (II)-porphyrin complexes [282, 336], rhodamine, chlorophyll [336], β-carotene [337, 338], tetracene, pentacene, and anthracene [339].

Chemical elements other than iodine, caesium, and carbon usually form nanowires, clusters, and/or nanocrystals in SWCNT channels. Also introduced into nanotube channels were nonmetals (elemental S, Se, Te [340, 341]) and metals including alkali metals (K [342]), p-metals (Bi [343]), transition metals (Fe [344, 345], Co [334], Ru [15], Pd [346], Ag [346–352], Cu [347, 353], Re [354–356], Au [346], Pt [346], W [354, 356], Os [354, 356]), and lanthanides (Eu [357, 358] and Er [359]).

Chemical compounds make up the largest group of dopants incorporated into SWCNT channels. They attract great interest for several reasons. First of all, the possibility of varying the chemical nature of cations and anions of salts markedly increases their number suitable for encapsulation,

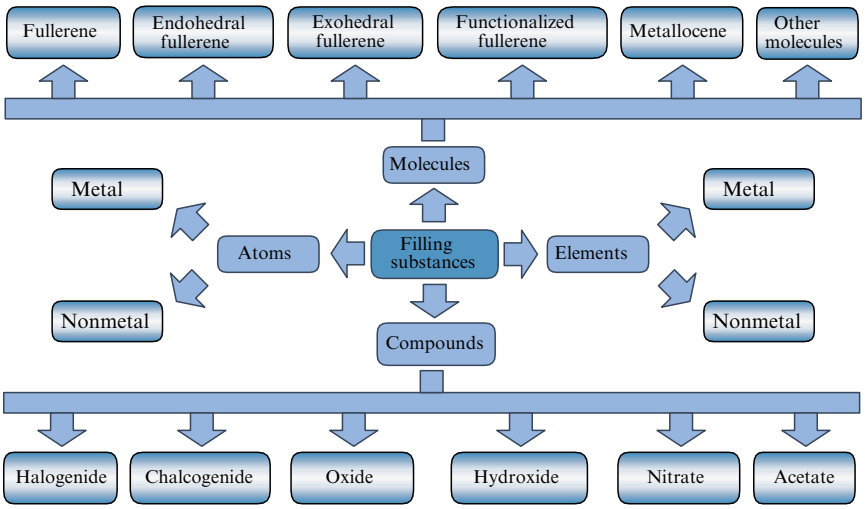

Figure 7. Classification of filling substances for SWCNTs by chemical nature.

Table 1. Classification of SWCNT-filling materials by chemical nature.

Type of material	Chemical nature		Examples	References
Atoms	Nonmetal		I_2	[203, 271, 272]
			$C_{10}H_2$	[275]
	Metal		Cs	[273, 274]
	Metal/nonmetal		Cs/I	[408]
Molecules	Fullerene		C_{60}, C_{70}, C_{78}, C_{80}, C_{82}, C_{90}	[14, 216, 276 – 294]
	Azafullerene		$C_{59}N$	[409]
	Doped fullerene		C_{60}/K	[410 – 412]
			$C_{60}/FeCl_3$	[412]
	Endohedral fullerene	$M@C_{82}$	Ca@C_{82}, La@C_{82}, Ce@C_{82}, Sm@C_{82}, Gd@C_{82}, Dy@C_{82}	[279, 284, 287, 295 – 302]
		$M_2@C_{80}$	$La_2@C_{80}$, $Ti_2@C_{80}$	[303, 304]
		$M_2@C_{84}$	$Sc_2@C_{84}$	[305]
		$M_2@C_{92}$	$Gd_2@C_{92}$	[306]
		$M_3N@C_{80}$	$Sc_3N@C_{80}$, $Dy_3N@C_{80}$, $Er_3N@C_{80}$, $Er_xSc_{3-x}N@C_{80}$	[283, 307 – 309]
		$X@C_{60}$	N@C_{60}	[289]
	Exohedral fullerene		$C_{60}O$	[310]
			$C_{60}Cs$	[311]
			C_{60}/Re, Os carbonyl complexes	[312 – 314]
	Fullerene containing functional group		$C_{61}(COOH)_2$, $C_{61}(COOC_2H_5)_2$	[283, 315]
			C_{60} with alkyl chains	[316]
			C_{60} with Cd organic complex	[317]
	Endohedral fullerene containing functional group		$Sc_3N@C_{80}$ with organic groups	[307]
	Metalocene		Ferrocene $(C_5H_5)_2Fe$	[318 – 329]
			Cobaltocene $(C_5H_5)_2Co$, $(C_5H_4C_2H_5)_2Co$	[330]
			Cerocene $(C_5H_5)_3Ce$	[331, 332]
	Metal acetylacetonate		$Pt(acac)_2$	[329, 333]
			$Co(acac)_2$	[334

Table 1. (Continued)

Type of material	Chemical nature			Examples	References
Molecules	Other organic molecules			Orthocarborane	[335]
				Zn(II), Pt(II) porphyrine complexes	[282, 336]
				Rhodamine, chlorophyll	[336]
				β-carotene	[337, 338]
				TDAE [1], TMTSF [2], TTF [3], DNBN [4], TCNQ [5], F_4TCNQ [6]	[339]
				Pentacene, anthracene	[339]
Elements (in the form of nanowires, clusters or nanocrystals)	Nonmetal			S, Se, Te	[340, 341]
	Metal	Alkali metal		K	[342]
		p-metal		Bi	[343]
		d-metal	3d	Fe	[344, 345]
				Co	[334]
				Cu	[347, 353]
			4d	Ru	[15]
				Pd	[346]
				Ag	[346 – 352]
			5d	Re	[354 – 356]
				Au, Pt	[346]
				W, Os	[354, 356]
		Lanthanide		Eu	[357, 358]
				Er	[359]
Compounds	Halogenide	Fluoride		SnF_2	[360]
		Chloride	$M^{I}Cl$	(Na/Cs/Cu/Ag/Tl)Cl	[61, 351, 361 – 364]
			$M^{II}Cl_2$	(Fe/Co/Ni/Mn/Pd/Zn/Cd)Cl_2	[61, 346, 364 – 370]
			$M^{III}Cl_3$	(Fe/Y/Ru/Au/La/Nd/Sm/Eu/Gd/Tb/Ho/Er/Yb)Cl_3, Al_2Cl_6	[15, 61, 344 – 346, 359, 364, 365, 370 – 373]
			$M^{IV}Cl_4$	(Zr/Hf/Pt/Th)Cl_4	[346, 364, 370, 374 – 377]

Table 1. (Continued)

Type of material	Chemical nature			Examples	References
Compounds	Halogenide	Chloride	$M^{V}Cl_5$	$MoCl_5$	[61]
			$M^{VI}Cl_6$	WCl_6	[61, 364]
			Mixture	$(KCl)_x(UCl_4)_y$	[351, 378]
		Bromide	$M^{I}Br$	(Cs/Cu/Ag)Br	[351, 361, 362, 364]
			$M^{II}Br_2$	(Fe/Co/Ni/Mn/Zn)Br_2	[366–369, 379]
		Iodide	$M^{I}I$	(Li/Na/K/Rb/Cs/Cu/Ag)I	[361, 362, 364, 375–378, 380–387]
			$M^{II}I_2$	(Ca/Sr/Ba/Fe/Co/Zn/Cd/Pb)I_2	[368, 369, 375–377, 388–390]
			$M^{III}I_3$	LaI_3, Al_2I_6	[370, 391, 392]
			$M^{IV}I_4$	SnI_4	[61, 364]
		Mixed		$AgCl_{0.2}Br_{0.8}$	[351]
				$AgCl_{1-x}I_x$	[364, 378, 393]
				$AgCl_xBr_yI_z$	[61, 351, 375, 380]
	Chalcogenide	$A^{II}B^{VI}$		HgTe	[394, 395]
				CdS, ZnTe	[396]
		$A^{IV}B^{VI}$		PbTe	[396]
				SnSe	[376]
				SnTe	[397, 398]
		$A^{IV}B_2^{VI}$		MoS_2	[399]
		$A^{VII}B_2^{VI}$		$MnTe_2$	[400, 401]
	Halogenide/chalcogenide			$CdBr_{2-x}Te_x$	[375]
	Oxide			PbO	[402]
				Sb_2O_3	[403, 404]
				Cr_2O_3	[405]
				UO_2	[406]
				CrO_3	[350, 407]
				Re_xO_y	[355]
	Hydroxide			CsOH, KOH	[406]
	Nitrate			$AgNO_3$	[346–350, 352]
				$Cu(NO_3)_2$	[347, 353]
				$Bi(NO_3)_3$	[343]
				$UO_2(NO_3)_2$	[406]

Table 1. (Continued)

Type of material	Chemical nature	Examples	References
Compounds	Acetate	$UO_2(CH_3COO)_2$	[406]
Mixed	Atoms/molecules	Cs/C_{60}	[408]
	Molecules/compounds	C_{60}/FeI_2	[364]
		$C_{60}/ThCl_4$	[364]

[1] TDAE — tetrakis(dimethylamino)ethylene
[2] TMTSF — tetramethyl-tetraselenfulvalene
[3] TTF — tetrathiafulvalene
[4] DNBN — 3,5-dinitrobenzonitryl
[5] TCNQ — tetracyano-p-quinodimethane
[6] F_4TCNQ — tetrafluorotetracyano-p-quinodimethane

as well as a versatility of their chemical and physical properties. Moreover, filling SWCNT channels with chemical compounds and their subsequent chemical modification make it possible to incorporate chemical elements that cannot be inserted through a one-step process.

Metal halogenides compose the biggest group of chemical compounds used to fill nanotube channels. SWCNT channels have been filled with various fluorides (SnF_2 [360]), chlorides ($M^{I}Cl$, where M = Na, Cs, Cu, Ag, Tl [61, 351, 361–364], $M^{II}Cl_2$, where M = Fe, Co, Ni, Mn, Pd, Zn, Cd [61, 346, 364–370], $M^{III}Cl_3$, where M = Fe, Y, Ru, Au, La, Nd, Sm, Eu, Gd, Tb, Ho, Er, Yb, Al_2Cl_6 [15, 61, 344–346, 359, 364, 365, 370–373], $M^{IV}Cl_4$, where M = Zr, Hf, Pt, Th [346, 364, 370, 374–377], $M^{V}Cl_5$, where M = Mo [61], $M^{VI}Cl_6$, where M = W [61, 364], $(KCl)_x(UCl_4)_y$ [351, 378]), bromides ($M^{I}Br$, where M = Cs, Cu, Ag [351, 361, 362, 364], $M^{II}Br_2$, where M = Fe, Co, Ni, Mn, Zn [366–369, 379]), iodides ($M^{I}I$, where M = Li, Na, K, Rb, Cs, Cu, Ag [361, 362, 364, 375–378, 380–387], $M^{II}I_2$, where M = Ca, Sr, Ba, Fe, Co, Zn, Cd, Pb [368, 369, 375–377, 388–390], $M^{III}I_3$, where M = La, Al_2I_6 [370, 391, 392], $M^{IV}I_4$, where M = Sn [61, 364]), and their mixtures ($AgCl_{0.2}Br_{0.8}$ [351], $AgCl_{1-x}I_x$ [364, 378, 393], and $AgCl_xBr_yI_z$ [61, 351, 375, 380]).

The second most popular group of encapsulating materials are metal chalcogenides $A^{II}B^{VI}$ (HgTe [394, 395], CdS [396], ZnTe [396]), $A^{IV}B^{VI}$ (PbTe [396], SnSe [376], SnTe [397, 398]), $A^{IV}B_2^{VI}$ (MoS_2 [399]), and $A^{VII}B_2^{VI}$ ($MnTe_2$ [400, 401]). Moreover, channels of SWCNTs have been filled with oxides (PbO [402], Sb_2O_3 [403, 404], Cr_2O_3 [405], UO_2 [406], CrO_3 [350, 407], Re_xO_y [355]), hydroxides (KOH, CsOH [406]), nitrates ($AgNO_3$ [346–350, 352], $Cu(NO_3)_2$ [347, 353], $Bi(NO_3)_3$ [343], $UO_2(NO_3)_2$ [406]), and acetates ($UO_2(CH_3COO)_2$ [406]). There are publications that report the simultaneous filling of SWCNT channels with atoms and molecules (Cs/C_{60} [408]) or molecules and chemical compounds (C_{60}/FeI_2, $C_{60}/ThCl_4$ [364]).

Naturally, the method of encapsulation of a filling material into SWCNTs depends on its chemical nature. Overall, compounds can be inserted into the channels in the gaseous, liquid, or solid state. Therefore, specific physical properties of a filling material can be of considerable importance, viz. solubility in a concrete solvent, melting, boiling, and decomposition points, surface tension coefficient and melt viscosity, vapor pressure at a given temperature, etc. On the one hand, the choice of material for filling nanotube channels is determined by the research goal and

limited by its properties and potential of the concrete filling technique. On the other hand, the development of novel filling methods for the purpose opens up new opportunities for the synthesis of new nanostructures.

The question of filling SWCNT internal channels by various methods is extensively discussed in the literature. Detailed reviews of the methods devised for encapsulating different materials can be found in Refs [61, 413–417].

5. Investigation of the electronic properties of filled SWCNTs

Interactions between an encapsulated material and a tube wall are mediated through the formation of local chemical bonds or nonlocal effects (e.g., charge transfer) [413]. In the latter case, the influence of incorporating materials on SWCNT electronic properties can be considered in the context of the rigid band model as the doping of nanotubes with the proper increase (donor doping) or decrease (acceptor doping) in the nanotube Fermi energy. In such cases, modification of the tube electronic structure due to accompanying charge transfer, alteration of work function, and shift of a Fermi level results in a change in SWCNT optical, transport, and electric properties.

Investigations into nanotube electronic properties aimed at detecting charge transfer, its direction, and local interactions between the encapsulated atoms and tube walls, as well as measurements of the work function of the filled SWCNTs and the shift of the Fermi level, can be conducted by such experimental methods as the aforementioned RS, XPS, XES, OAS, XAS, UPS, and PLS. The last four techniques directly yield information about modifications of van Hove singularities, a distinctive feature of the band structure of SWCNTs (see Section 3). Moreover, the electronic properties of SWCNTs can be studied by quantum-chemical simulation. Table 2 summarizes results of experimental and theoretical studies on the electronic properties of filled nanotubes.

5.1 Experimental investigation of the electronic properties of filled SWCNTs

The literature contains publications on the qualitative (detection of charge transfer and its direction) and quantitative (measurement of the work function, determination of the Fermi level position and its displacement with respect to the initial position) analysis of the modification of SWCNT electronic properties using experimental methods. In what follows, the reported studies on electronic properties of filled SWCNTs by experimental techniques will be considered.

5.1.1 Detection of charge transfer and its direction. The detection of charge transfer and the determination of its direction at the qualitative level can be performed by optical absorption spectroscopy, Raman spectroscopy, photoluminescence spectroscopy, and X-ray absorption spectroscopy.

Optical absorption spectroscopy. Optical absorption spectra of SWCNTs show characteristic peaks in an energy range from 0.5 to 3 eV, corresponding to electron transitions between van Hove singularities of semiconducting and metallic SWCNTs (Fig. 8a). The distance between van Hove singularities of the conduction and valence bands being inversely proportional to SWCNT diameter, the energy position of the peaks differs for nanotubes of various diameters [418]. According to the Kataura plot (Fig. 8b), the peak in the 0.6–0.8 eV region for SWCNTs 1.4–1.6 nm in diameter corresponds to transition E_{11}^{S} between the first van Hove singularities of semiconducting nanotubes, the peak in the 1.0–1.4 eV region to transition E_{22}^{S} between the second van Hove singularities of semiconducting nanotubes, the peak in the 1.7–2.0 eV region to transition E_{11}^{M} between the first van Hove singularities of metallic nanotubes, and the peak in the 2.3–2.5 eV region to transition E_{33}^{S} between the third van Hove singularities of semiconducting nanotubes [44].

Modification of OA spectra, e.g., variation of peak intensity and position, may reflect changes in electronic properties of SWCNTs. The literature contains reports of OA spectra of SWCNTs filled with organic [339] and metallorganic [322, 330] molecules, and halogenides of iron [369], cobalt [379], nickel [366], manganese [367], zinc [368], silver [361], and copper [362]. The authors of these studies observed both a decrease [339] and an increase [322, 330] in the intensity of the peak of the first van Hove singularity in semiconducting SWCNTs or its complete disappearance [361, 362, 366–369, 379]. It was therefore concluded that charge transfer occurs in filled nanotubes (see Table 2) even if its direction cannot be determined by the method in question.

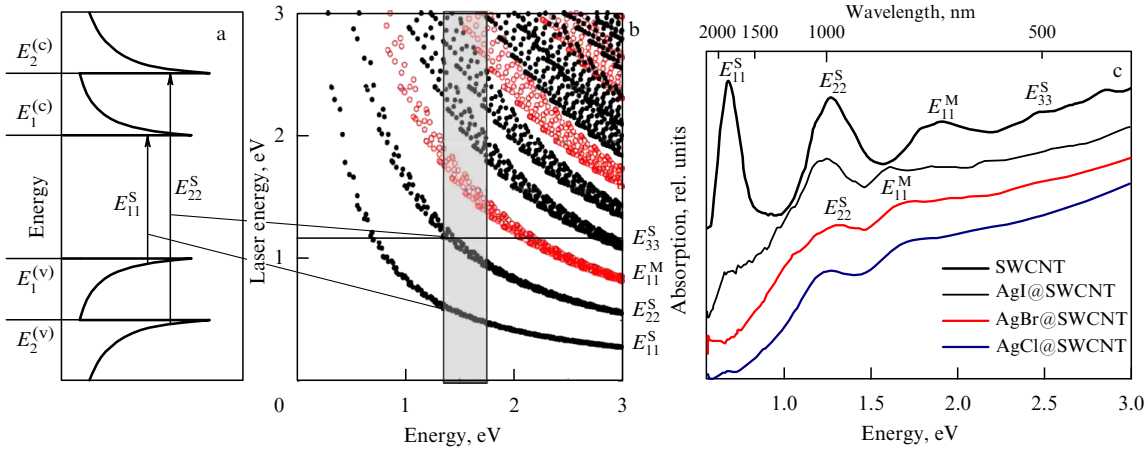

Figure 8. (a) Schematic of the band structure of semiconducting SWCNTs, (b) Kataura plot: dependence of electron transition energy between van Hove singularities on nanotube diameter (the plot shows the region corresponding to SWCNTs 1.4–1.6 nm in diameter) [44], and (c) optical absorption spectra of pristine and silver halogenide-filled nanotubes [361].

Table 2. Investigations of the electronic properties of filled SWCNTs using experimental and theoretical methods.

Observed effect	Encapsulated material	Method	Result	References
Charge transfer from SWCNT wall	C_{60}	XAS	Slightly modified shape of the C1s-spectrum and altered intensity of the components suggest small charge transfer from SWCNT walls to encapsulated C_{60} molecules.	[432]
		UPS	SWCNT spectra before and after filling are identical.	[288]
		Quantum-chemical calculations	Changes in electronic properties of SWCNTs depend on their diameter. For example, nanostructures resulting from the encapsulation of molecules into SWCNTs more than 1.18 nm in diameter were characterized by a small charge transfer from SWCNT walls to C_{60} molecules, whereas after filling of SWCNTs less than 1.18 nm in diameter charge transfer from C_{60} molecules to tube walls occurred.	[437 – 442]
	C_{70}, C_{78}, C_{82}	Quantum-chemical calculations	Changes in electronic properties of SWCNTs depend on their diameter. Charge transfer from tube walls occurred in (17, 0) SWCNTs filled with C_{82} molecules.	[439 – 441]
	CrO_3	RS	A shift of G-mode peaks to the high-energy region; the G-mode shape changes to the semiconducting type.	[350]
		Quantum-chemical calculations	Calculations of the band structure suggest acceptor doping of SWCNTs.	[454]
	CuI	RS	A shift of G-mode peaks to the low-energy region; the G-mode shape changes to the semiconducting type.	[381]
		RS	A shift of G-mode peaks to the high-energy region; the G-mode shape changes to the semiconducting type.	[385]
	S, Se, Te	RS	A shift of G-mode peaks to the high-energy region.	[341]
	SnF_2	RS	A shift of G-mode peaks to the high-energy region.	[360]
	Organic molecules (tetracene, pentacene, anthracene, TDAE,[1] TMTSF,[2] TTF,[3] DNBN,[4] TCNQ,[5] F_4TCNQ[6])	OAS, RS	Altered relation between intensities of components of G-mode peaks in Raman spectra and lowered intensity of the peak corresponding to electron transitions between the first van Hove singularities of semiconducting nanotubes in OAS spectra give evidence of charge transfer. Charge transfer from SWCNT walls to encapsulated molecules is proved for TCNQ.	[339]
		Quantum-chemical calculations	Encapsulation of TCNQ and F_4TCNQ electrophilic molecules results in acceptor doping of SWCNTs.	[443]
	Gd@C_{82}	XPS, UPS, XAS	A shift of C1s XPS peak to the high-energy region and its broadening due to charge transfer from SWCNT walls. Heating of Gd@C_{82}@SWCNT nanostructures results in formation of metallic Gd inside DWCNTs, a shift of C1s XPS spectrum to the low-energy region, and the loss of van Hove singularity signal in C1s XAS spectrum. The XPS spectrum of this specimen is characterized by the enhanced density of electron states at the Fermi level, suggesting donor doping of SWCNTs.	[301]
	La@C_{82}, K@C_{60}, Ca@C_{60}, Y@C_{60}	Quantum-chemical calculations	The efficiency of charge transfer from SWCNT walls to dopant molecules is higher than for C_{60}.	[437, 439]
	KI	Quantum-chemical calculations	Charge transfer from SWCNT walls to the nanocrystal turns to be very small.	[456]
	AgCl, AgBr, AgI	OAS, RS, RS with electrochemical charging, XAS , XPS	OAS spectra evidence the loss of the peak corresponding to electron transitions between the first van Hove singularities of semiconducting SWCNTs. Raman spectra undergo a shift of G-mode peaks to the high-energy region; the G-mode shape changes to the semiconducting type. According to RS with electrochemical charging, the Fermi level of AgI-filled SWCNTs shifts downward by 0.6 eV. C1s XAS spectrum has an additional peak on the low-energy side of π^* resonance, which corresponds to the appearance of a new unoccupied level due to charge transfer from SWCNT walls. XPS spectrum contains additional components. Charge transfer increases in the AgI–AgBr–AgCl line. Local interaction presumably occurs, but its nature is unknown.	[361]

Table 2. (Continued)

Observed effect	Encapsulated material	Method	Result	References
Charge transfer from SWCNT wall	$FeCl_2$, $FeBr_2$, FeI_2	OAS, RS, XAS, XPS	Peak corresponding to electron transitions between the first van Hove singularities of semiconducting SWCNTs disappears in OAS spectra. Raman spectra undergo a shift of G-mode peaks to the high-frequency region; G-mode shape changes to the semiconducting type. C1s XAS spectrum has an additional peak on the low-energy side of π^* resonance, which corresponds to the appearance of a new unoccupied level due to charge transfer from SWCNT walls. XPS spectrum contains additional components.	[369]
	$CoBr_2$	OAS, RS, XPS	OAS spectra evidence the loss of the peak corresponding to electron transitions between the first van Hove singularities of semiconducting SWCNTs. Raman spectra undergo a shift of G-mode peaks to the high-energy region; the G-mode shape changes to the semiconducting type. XPS spectrum contains additional components.	[379]
	$NiCl_2$, $NiBr_2$	OAS, RS, XAS, XPS	Peak corresponding to electron transitions between the first van Hove singularities of semiconducting SWCNTs disappears in OAS spectra. Raman spectra undergo a shift of G-mode peaks to the high-frequency region; G-mode shape changes to the semiconducting type. C1s XAS spectrum has an additional peak on the low-energy side of π^* resonance, which corresponds to the appearance of a new unoccupied level due to charge transfer from SWCNT walls. XPS spectrum contains additional components.	[366]
	$MnCl_2$, $MnBr_2$	OAS, RS, XPS	OAS spectra evidence the loss of the peak corresponding to electron transitions between the first van Hove singularities of semiconducting SWCNTs. Raman spectra undergo a shift of G-mode peaks to the high-energy region; the G-mode shape changes to the semiconducting type. XPS spectrum contains additional components.	[367]
	$ZnCl_2$, $ZnBr_2$, ZnI_2	OAS, RS, XAS, XPS, measurement of work function, UPS	Peak corresponding to electron transitions between the first van Hove singularities of semiconducting SWCNTs disappears in OAS spectra. Raman spectra undergo a shift of G-mode peaks to the high-frequency region; G-mode shape changes to the semiconducting type. C1s XAS spectrum has an additional peak on the low-energy side of π^* resonance, which corresponds to the appearance of a new unoccupied level due to charge transfer from SWCNT walls. XPS spectrum contains additional components. Measurements of work function show that it equals 4.76 eV for pristine SWCNTs, and 5.14 eV for $ZnBr_2$-filled nanotubes. The valence band spectrum of filled nanotubes shows a shift of π^* resonance to the low-frequency region by 0.26 eV, corresponding to a shift of the Fermi level in filled SWCNTs.	[368]
	$TbCl_3$, $ZnCl_2$, $CdCl_2$	OAS, RS, XPS	OAS spectra evidence the loss of the peak corresponding to electron transitions between the first van Hove singularities of semiconducting SWCNTs. Raman spectra undergo a shift of G-mode peaks to the high-energy region; the G-mode shape changes to the semiconducting type. XPS spectrum contains additional components.	[365]
Charge transfer to SWCNT wall	Ag	RS	A shift of G-mode peaks to the low-energy region, broadening of the G-band, G-mode shape changes to the metallic type.	[350]
		OAS, RS, XPS	A shift of G-mode peaks to the low-energy region, broadening of the G-mode peak, G-mode shape changes to the metallic type. XPS spectrum contains additional components.	[347, 348]
		Quantum-chemical calculations	Calculations of the band structure suggest donor doping of SWCNTs.	[454, 455]
	Cu	RS, XPS	A shift of G-mode peaks to the low-energy region, broadening of the G-mode peak, G-mode shape changes to the metallic type. XPS spectrum contains additional components.	[347, 353]
	Organic molecules (tetracene, pentacene, anthracene, TDAE, TMTSF, TTF, DNBN, TCNQ, F_4TCNQ)	OAS, RS	Altered relation between intensities of components of G-mode peaks in Raman spectra and lowered intensity of the peak corresponding to electron transitions between the first van Hove singularities of semiconducting nanotubes in OAS spectra give evidence of charge transfer. Charge transfer from encapsulated molecules to SWCNT walls is proved for TMTSF and TTF.	[339]
		Quantum-chemical calculations	Encapsulation of TDAE and TTF nucleophilic molecules into SWCNT channels results in donor doping of nanotubes.	[443]

Table 2. (Continued)

Observed effect	Encapsulated material	Method	Result	References
Charge transfer to SWCNT wall	$Co(C_5H_5)_2$, $Co(C_5H_4C_2H_5)_2$	OAS , PLS	A shift of peaks in PL spectra of filled SWCNTs to the low-energy region along the emitted radiation energy axis suggests formation of impurity levels below the conduction band. Enhanced intensity of the peaks positioned at energies below 1 eV in OAS spectra.	[330]
		Quantum-chemical calculations	Filling (17, 0) and (12, 0) nanotubes results in charge transfer from $Co(C_5H_5)_2$ molecules onto SWCNT walls.	[444, 445]
	$Fe(C_5H_5)_2$	UPS	A shift of peaks of the first and second van Hove singularities in semiconducting SWCNTs and of the first singularity in metallic SWCNTs by 0.1 eV to the high-energy region.	[328]
		XPS, UPS, XAS , quantum-chemical calculations	Broadened and more asymmetric C1s XPS spectrum. Decreased intensity of π^* resonance in C1s XAS spectrum. Van Hove singularity peaks in UPS spectra are shifted toward the higher binding energies, which suggests charge transfer to SWCNT walls. Heating of the sample causes decomposition of ferrocene accompanied by a shift of van Hove singularity peaks in the opposite direction down to values below those in pristine SWCNTs, i.e., the type of doping switches from donor to acceptor. Estimated charge transfer density is $0.0067\,e^-\,Å^{-1}$ for ferrocene-filled SWCNTs, and is $0.001\,e^-\,Å^{-1}$ for the sample annealed at 600 °C for 8 h. Quantum-chemical calculations showed that charge transfer density for ferrocene-filled (9, 9) SWCNTs is 0.002 and $0.0029\,e^-\,Å^{-1}$ for perpendicular and linear orientations of the molecules in the nanotube channel, respectively.	[326]
		XPS, UPS, XAS	Broadened C1s XPS spectrum. Decreased intensity of the component of the first van Hove singularity in C1s XAS spectrum corresponds to donor doping of SWCNTs. The shape of Fe2p XAS spectrum suggests a change in the oxidation level of iron to $Fe^{2.1+}$ due to charge transfer. UPS spectrum does not change because of a low filling degree of SWCNT channels.	[324]
		OAS, PLS, quantum-chemical calculations	Increased intensity of the peak corresponding to electron transitions between the first van Hove singularities of semiconducting SWCNTs is observed in the OAS spectrum. Photoluminescence spectrum shows increased intensity of the signal for (8, 6) and (9, 5) SWCNTs ($d \approx 0.9$ nm) due to charge transfer to SWCNT walls. Quantum-chemical calculations implied that charge transfer density is $0.0119\,e^-\,Å^{-1}$ for (8, 6) SWCNTs, $0.0124\,e^-\,Å^{-1}$ for (9, 5) SWCNTs, and $0.0106\,e^-\,Å^{-1}$ for (16, 0) SWCNTs.	[322]
		Quantum-chemical calculations	Filling (17, 0) and (12, 0) nanotubes results in charge transfer from $Fe(C_5H_5)_2$ molecules to SWCNT walls.	[444, 445]
	$Ce(C_5H_5)_3$	XPS, UPS, XAS	Decreased intensity of the component of the first van Hove singularity of semiconducting SWCNTs in C1s XAS spectrum. Broadened and more asymmetric C1s XPS spectrum, suggesting donor doping of SWCNTs. UPS spectrum of annealed cerocene-containing nanotubes is characterized by enhanced density of electron states at the Fermi level, which suggests increased donor doping level.	[331, 332]
	$M(C_5H_5)_2$, where M = V, Cr, Mn, Ni	Quantum-chemical calculations	Calculations of the band structure give evidence of SWCNT doping upon filling their channels.	[444]
	Eu	XPS, UPS, XAS	Decreased intensity of components of van Hove singularities of semiconducting SWCNTs SWCNTs in C1s XAS spectrum. Shift of C1s peak in XPS spectrum toward higher binding energies and its broadening. Shift by 0.1 eV of van Hove singularity peaks in UPS spectrum to the high-energy region. Increased density of electron states at the Fermi level in UPS spectrum, which suggests donor doping of SWCNTs. Number of transferred electrons is 1.79 per Eu atom.	[358]
		Quantum-chemical calculations	Calculations of the band structure of filled (10, 0) and (6, 0) nanotubes give evidence of donor doping of SWCNTs.	[451]
	Li, K	Quantum-chemical calculations	Calculations of the band structure of filled $[Li@C_{24}]_n$ and $[K@C_{36}]_n$ tubulenes give evidence of charge transfer from the nanotube walls to the encapsulated metallic atoms.	[436]

Table 2. (Continued)

Observed effect	Encapsulated material	Method	Result	References
Charge transfer to SWCNT wall	Ti, Zn, Co, Ni, Fe, Mo, Gd, Cu	Quantum-chemical calculations	Calculations of the band structure and the density of electron states of filled nanotubes with different chiral vectors give evidence of donor doping of SWCNTs.	[446 – 453]
Local interaction and charge transfer	Ag	XAS	Appearance of additional peak between π^* and σ^* resonances in the C1s spectrum reflects hybridization of carbon and silver valence orbitals. Decreased intensity of the π^*-peak may indirectly suggest charge transfer from silver atoms to carbon atoms of nanotube walls.	[345]
	$ErCl_3$	XPS, UPS, XAS	Broadening of C1s XPS spectrum up to 0.2 eV, its shift toward lower binding energies, and appearance of additional peak on the low-energy side suggest hybridization of erbium 5d-orbitals and carbon π-orbitals. Sample annealing with formation of Er clusters in SWCNT channels causes reverse shift of Cls peak and its narrowing. C1s XAS spectrum of annealed sample shows increased intensity of components of van Hove singularities located on the low-energy side from π^* resonance; this suggests increased charge transfer as confirmed by resonant UPS for Er 3d and 4d levels.	[359]
	CuCl, CuBr, CuI	XAS, XES, OAS, RS, RS with electrochemical charging, XPS, measurement of work function, UPS	The appearance of additional peaks in C1s and Cu2p XAS spectra and modification of the Cu $K\beta_5$ RES spectrum suggest the formation of a new localized level due to hybridization between $2p_z$ π-orbitals of carbon and 3d-orbitals of copper. The energy position of this peak is virtually independent of the type of the halogen atom, while the density of electron states at this level increases in the CuI–CuBr–CuCl series. OAS spectra evidence the loss of the peak corresponding to electron transitions between the first and the second (in the case of CuCl) van Hove singularities of semiconducting SWCNTs. In Raman spectra, the G-mode peaks shift to the high-energy region, while the G-mode shape changes to the semiconducting type. According to results of RS with electrochemical charging, the Kohn anomaly is also displaced, which corresponds to the shift of the Fermi level in SWCNTs (by −0.3 eV for CuI, and −0.75 eV for CuCl). Because copper halogenides cannot accept electrons, charge transfer occurs from SWCNT walls to the new localized level. Measurements of the work function show that it equals 4.6 eV for pristine SWCNTs, 4.8, 5.2, and 5.25 eV for nanotubes filled with CuI, CuBr, and CuCl, respectively. The valence band spectrum of filled nanotubes exhibits a shift of π^* resonance to the low-energy region by 0.2 eV for CuI, 0.6 eV for CuBr, and 0.7 eV for CuCl; these values correspond to the displacement of the Fermi level in filled SWCNTs. The XPS spectrum contains additional components whose shift increases in the CuI–CuBr–CuCl series. Thus, charge transfer occurs with the participation of the newly formed localized levels; moreover, acceptor doping of SWCNTs takes place due to the difference in the work function between SWCNTs and encapsulated copper halogenides.	[362]
No effect on electronic properties	SnTe	RS, OAS, XPS	Similar SWCNT spectra before and after filling.	[397]
	β-carotene	RS, OAS	Similar SWCNT spectra before and after filling.	[338]

[1] TDAE — tetrakis(dimethylamino)ethylene, [2] TMTSF — tetramethyl-tetraselenfulvalene, [3] TTF — tetrathiafulvalene, [4] DNBN — 3,5-dinitrobenzonitryl, [5] TCNQ — tetracyano-p-quinodimethane, [6] F_4TCNQ — tetrafluorotetracyano-p-quinodimethane.

Figure 8c shows OA spectra of pristine nanotubes and SWCNTs filled with silver halogenides [361].

Raman spectroscopy. Raman spectra of SWCNTs are characterized by the presence of three features, viz. the radial breathing mode (RBM) at frequencies < 200 cm^{-1} corresponding to synchronous radial vibrations of carbon atoms (A_{1g}), high-frequency G-band between 1500 and 1600 cm^{-1} related to vibrations of the C–C bond (E_{2g} vibrations of the graphene layer), and D-line in the 1300–1350 cm^{-1} region related to structural defects and disordering, along with the second-order modes in the 2400–3000 cm^{-1} region [419].

The position of RBM peaks in the Raman spectrum is inversely proportional to SWCNT diameter [36, 419–422]. The use of lasers with various energies makes it possible to detect SWCNTs of different diameters. Therefore, the analysis of RBM band permits assessing the diameter distribution of nanotubes [420, 422].

The G-region of SWCNT Raman spectra is characterized by the two most intense modes, G^- and G^+ [421]. For semiconducting nanotubes, the G^- mode is related at low frequencies ($\sim$ 1540–1575 cm^{-1}) to tangential vibrations (at a tangent along the nanotube perimeter) of carbon atoms, and the G^+ mode at high frequencies ($\sim$ 1590 cm^{-1}) to longitudinal (along the SWCNT axis) vibrations. On the other hand, the inverse relationship takes place for metallic nanotubes due to electron–phonon interaction [423]. This

accounts for a marked difference between G-mode profiles of semiconducting and metallic nanotubes. In the former case, the G-mode shows up a narrow symmetric peak described by the Lorentz function; in the latter case, the G-mode has a wide asymmetric shape described by the Breit–Wigner–Fano (BWF) function [419, 424).

Modification of the Raman spectrum, specifically the shift of G-mode peaks and a change in the mode profile, may reflect changes in SWCNT electronic properties. Therefore, the measurement of the Raman spectra of filled SWCNTs at different laser energies, making it possible to reach resonant conditions of excitation of nanotubes differing in diameter and conduction type, is an important tool for investigating the electronic properties of filled SWCNTs.

The reports are issued describing Raman spectra of SWCNTs filled with CrO_3 [350], CuCl, CuBr, CuI [362, 381, 385], S, Se, Te [341], SnF_2 [360], organic molecules [339], $FeCl_2$, $FeBr_2$, FeI_2 [369], $CoBr_2$ [379], $NiCl_2$, $NiBr_2$ [366], $MnCl_2$, $MnBr_2$ [367], $ZnCl_2$, $ZnBr_2$, ZnI_2 [365, 368], $CdCl_2$ [365], $TbCl_3$ [365], AgCl, AgBr, AgI [361], Ag [347, 348, 350], Cu [347, 353], SnTe [397], and β-carotene [338] (see Table 2).

The authors of the above-mentioned papers observed modification of RBM peaks along with the displacement of G-mode peaks and changes in the mode profile. In early studies [341, 350, 360, 381], the shift of G-mode peaks to the higher-frequency region was attributed to charge transfer from nanotube walls, while the low-frequency shift was related to charge transfer to SWCNT walls. Based on these evidences it was concluded that CrO_3 [350], S, Se, Te [341], CuI [381, 385], and SnF_2 [360] are electron acceptors, while Ag [350] is a donor of electrons. The authors of Ref. [350] noted that this conclusion is confirmed by measurements of SWCNT Raman spectra under electrochemical charging [236], but a paper published in 2008 [425] demonstrated that application of positive potentials to SWCNTs (analogous to donor-type doping of nanotubes) may cause a shift of G-mode peaks to the high-frequency region of the Raman spectrum. This was probably the reason why the authors of later studies [347, 348, 353, 361, 362, 365–369, 379, 397] could not come to a conclusion as regards the direction of charge transfer based on the RS data alone. Figure 9 presents the Raman spectra of SWCNTs filled with S, Se, and Te [341].

Photoluminescence spectroscopy. When a semiconducting SWCNT is laser irradiated with a photon energy sufficient to initiate electron transition between the second van Hove singularities of the valence and conduction bands, an electron enters the conduction band. As it returns to the valence band by means of transition between the first van Hove singularities, it emits radiation (Fig. 10a) [426–428].

Photoluminescence spectra maps reflecting the two-dimensional dependence of photoluminescence intensity on the wavelengths of exciting and emitted radiation show up separate points (Fig. 10b, c). The width of the SWCNT bandgap being dependent on its structure and inversely proportional to nanotube diameter, each such point corresponds to an SWCNT of a definite chirality [426, 427].

Modification of PL spectra, such as variation of PL intensity for nanotubes of definite chirality, and displacement of the points corresponding to these tubes along the axes of exciting and emitted radiation wavelengths may indicate changes in the electronic properties of SWCNTs. Moreover, this observation permits estimating the effectiveness of filling SWCNTs of a given chirality with the selected substance.

There are known in literature only a few studies on PL spectra of filled nanotubes (see Table 2). The authors of Ref. [322] recorded PL spectra of ferrocene-filled SWCNTs and showed that the molecules are incorporated only into nanotubes having the chiral vectors (8, 6), (9, 5), (8, 7), (11, 1), and (10, 5). The comparison of PL maps of pristine (Fig. 10b) and filled (Fig. 10c) SWCNTs revealed signal enhancement by 170% and 270% for (8, 6) and (9, 5) SWCNTs, respectively. Moreover, the authors observed a red shift of PL peaks along the axis of the emitted radiation wavelength. From the above evidences it was concluded that charge transfer from ferrocene molecules to SWCNT walls took place.

X-ray absorption spectroscopy. C1s XAS spectra of SWCNTs, which were recorded upon initiation of electron transitions from the C1s core level to the conduction band of nanotubes by exposure of the sample to synchrotron radiation, show two main peaks [429]. One of them is π^* resonance

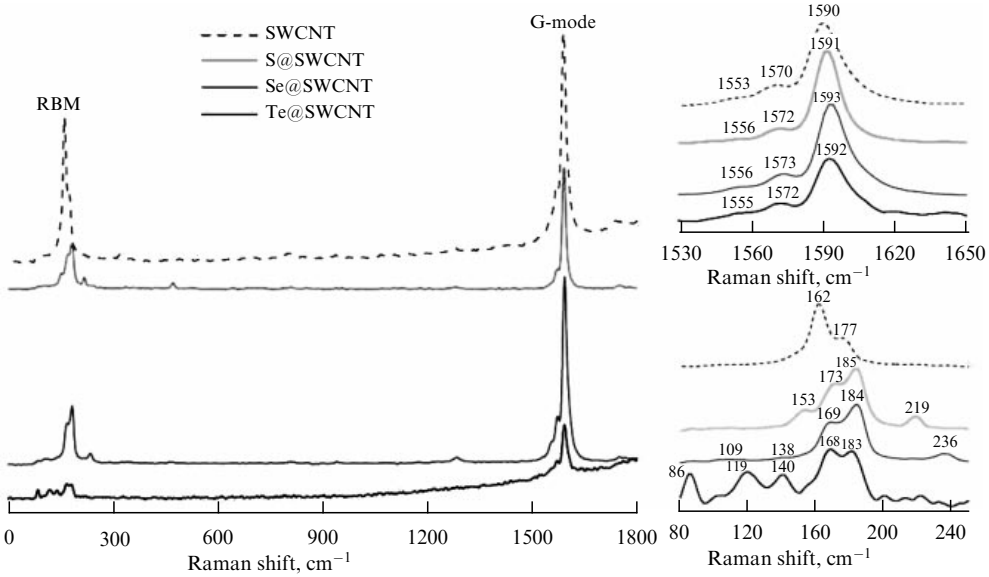

Figure 9. Results of Raman spectroscopic studies for SWCNTs filled with elemental sulfur, selenium, and tellurium [341].

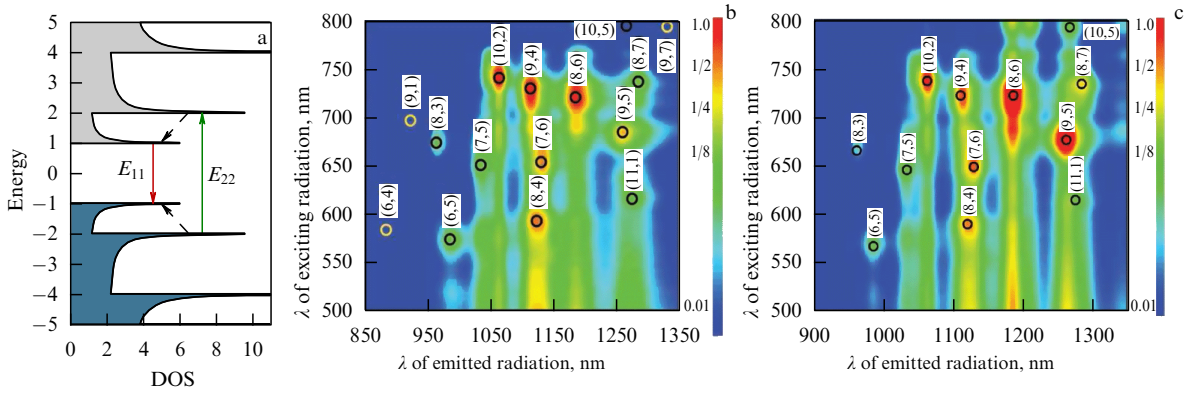

Figure 10. (Color online.) Schematic representation of the photoluminescence process (a) [426] and the photoluminescence maps of pristine nanotubes (b) and SWCNTs filled with ferrocene molecules (c) [322].

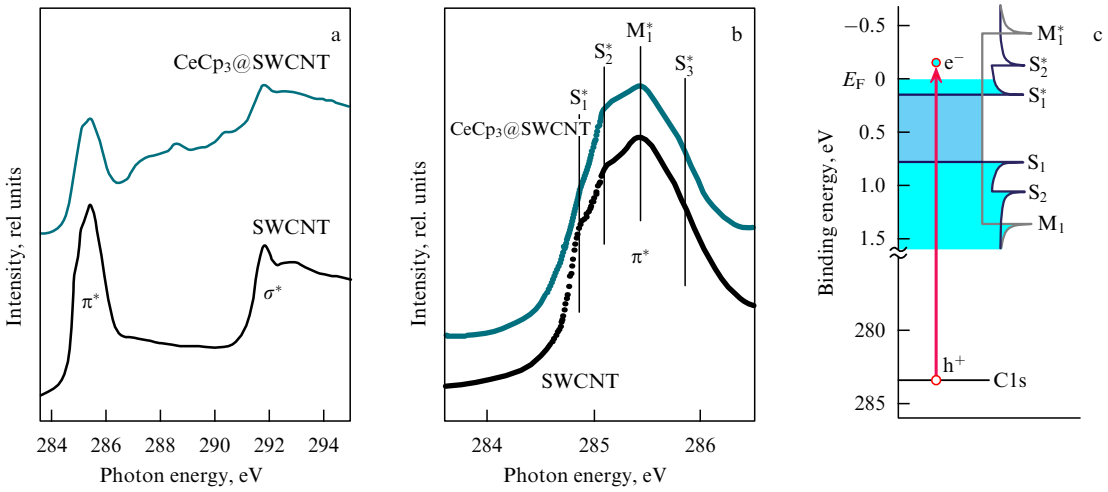

Figure 11. (a, b) C1s X-ray absorption spectra of pristine and cerocene–filled nanotubes [332], and (c) schematic of electron transition from the C1s core level to the conduction band of doped SWCNTs [331].

located at an energy of 285.5 eV, which corresponds to electron transition into the π^*-band of SWCNTs. The other peak relates to σ resonance located at 291.8 eV and corresponds to electron transition into the σ^*-band of nanotubes (Fig. 11a). The presence of these two peaks is characteristic of C1s XAS spectra for all allotropic modifications of carbon with sp^2-hybridization of the atoms; it was thoroughly investigated for graphite in Ref. [430].

High-resolution spectroscopic measurements make it possible to study the fine structure of π^* resonance for an SWCNT sample with narrow diameter distribution [431], with each peak corresponding to an electron transition from the C1s core level to individual van Hove singularities of the SWCNT conduction band (S_1, S_2, S_3 are the first, second, and third van Hove singularities of semiconducting SWCNTs, respectively, and M_1 is the first van Hove singularity of metallic nanotubes in Fig. 11b) [429].

Modification of C1s XAS spectra, specifically variation of intensity of π^* resonance components, corresponding to individual van Hove singularities, and regular changes of the π^*-resonance profile, the disappearance of its fine structure or the appearance of additional peaks near π^* resonance, may reflect changes in the electronic properties of SWCNTs. There are reports on the measurement of C1s XAS spectra of SWCNTs filled with C_{60} [432], Gd@C_{82} [301], AgCl, AgBr, AgI [361], CuCl, CuBr, CuI [362], $FeCl_2$, $FeBr_2$, FeI_2 [369], $NiCl_2$, $NiBr_2$ [366], $ZnCl_2$, $ZnBr_2$, ZnI_2 [368], Ag [345], $ErCl_3$ [359], Eu [358], ferrocene [324, 326], and cerocene [331, 332] molecules; the fine structure of π^* resonance was studied for the last four compounds (see Table 2).

C1s XAS spectra of SWCNTs filled with Ag [361], Cu [362], Fe [369], Ni [366], and Zn [368] halogenides contain an additional peak on the low-energy side from π^* resonance. In the case of Ag, the additional peak appears between π^*- and σ^*-resonances [345]. From these evidences it was concluded that charge transfer gives rise to a new level in the SWCNT band structure. As far as nanotubes filled with europium [358], ferrocene [324, 326], and cerocene [331, 332] are concerned, the authors observed in C1s XAS spectra a decrease in intensity of the component corresponding to the first van Hove singularity of semiconducting SWCNTs, which was attributed to donor doping of nanotubes by the filling agents. Figure 11a, b presents C1s XAS spectra of cerocene-filled nanotubes, and Fig. 11c shows schematically the electron transition from the C1s core level to the conduction band of doped nanotubes.

5.1.2 Elucidation of local interactions between the atoms of encapsulated substances and nanotube walls. Evaluation of their influence on SWCNT electronic properties. As shown above, if the interaction between an inserted substance and the nanotube wall is emerging, for example, through the

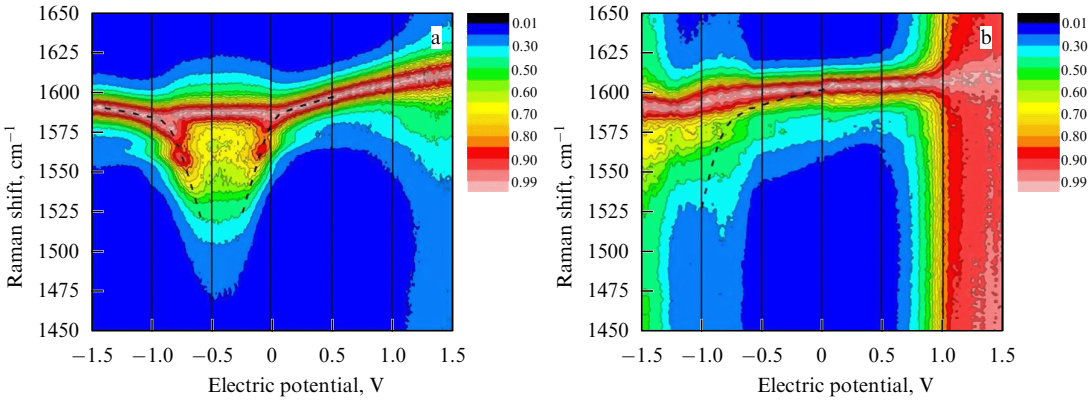

Figure 12. (Color online.) RS maps under electrochemical charging in the G-region for pristine SWCNTs (a) and CuCl@SWCNT nanocomposite (b), illustrating the shift of the Kohn anomaly upon filling SWCNT channels with copper chloride. The maps were normalized to maximum intensity in the 1450–1650 cm^{-1} region to improve image quality.

formation of local chemical bonds, then the modification of the SWCNT electronic properties cannot be considered in the framework of the rigid band model. The local interaction was reported to exist in nanotubes filled with erbium chloride [359], silver [345], and copper halogenides [362]. However, this does not mean that it is absent in all other aforementioned filled nanotubes simply because this matter was not dealt with by the authors of the cited works.

As mentioned above, the C1s XAS spectrum of silver-filled SWCNTs contains an additional peak between π^*- and σ^*-resonances, which the authors of Ref. [345] attributed to hybridization of the valence orbitals of carbon and silver and suggested the possibility of charge transfer from silver atoms to the wall of SWCNTs. The appearance of additional components in the C1s XAS spectrum of erbium chloride on the low-energy side of π^* resonance gave evidence of hybridization between 5d-orbitals of erbium and π-orbitals of carbon [359]. A rise in intensity of these components related to the enhancement of the degree of hybridization and charge transfer was observed during annealing of the sample with the formation of Er clusters in an SWCNT channel. This observation was confirmed by resonant UPS for the 3d and 4d levels of erbium.

Based on the results of XAS and XES studies of SWCNTs filled with copper halogenides, the authors of Ref. [362] postulated the formation of chemical bonds between the nanotube and the encapsulated salts by means of hybridization between $2p_z$ π-orbitals of carbon and 3d-orbitals of copper. This inference was supported by the appearance of additional peaks in C1s and Cu2p XAS spectra and modification of the Cu $K\beta_5$ XES spectrum as a result of the formation of a new localized level in the band structure of SWCNTs. The energy position of this level was practically independent of the type of halogen atoms, whereas the efficiency of charge transfer from nanotube walls to this localized level increased in the CuI–CuBr–CuCl series.

5.1.3 Determination of the shift of the SWCNT Fermi level upon filling of nanotube channels. Methods devised for studying the modification of SWCNT electronic properties at the qualitative level have been described in Sections 5.1.1 and 5.1.2. Determination of the Fermi level in filled nanotubes and its shift from the initial position are performed using RS under electrochemical charging, the measurement of SWCNT work function, UPS, and XPS.

Raman spectroscopy under electrochemical charging. As was mentioned in Section 4.5, electrochemical charging permits intentional modification of the electronic properties of nanotubes and control of the doping level [277]. The combination of electrochemical charging and RS enabled the authors of Refs [361, 362] to accurately determine the shift of the Fermi level in SWCNTs filled with silver iodide [361] and copper halogenides [362]. In the case of AgI, the shift was -0.6 eV [361], whereas for copper iodide and copper chloride it was -0.3 and -0.75 eV, respectively [362]. In both studies, charging was performed in a three-electrode electrochemical cell with an SWCNT-coated platinum electrode using a 0.2 M $LiClO_4$ solution in 1,2-dimethoxymethane as the electrolyte and applying potentials in the range of -1.5 to 1.5 V.

Raman spectroscopy maps showing the two-dimensional dependence of the intensity of G-mode peaks on the Raman shift and the applied potential for pristine and copper chloride-filled SWCNTs are represented in Fig. 12. The dependence of the G-mode peak position of pristine SWCNTs on the applied potential is characterized by the presence of two branches (Fig. 12a), one of which is displaced to the higher-frequency region at potentials greater than -0.35 V, and the other of which is independent of the applied potential, as is typical of armchair nanotubes [433]. Thus, the Kohn anomaly in the case of pristine SWCNTs is located at -0.35 V, and its shift toward negative potentials (from zero position) is attributed by the authors of Ref. [362] to the interaction between SWCNTs and electrolyte molecules.

The Raman spectroscopy map for copper chloride-filled SWCNTs presents a somewhat blurred picture along the direction of the applied potential (Fig. 12b). Nevertheless, the position of the Kohn anomaly is still possible to determine as -1.1 V. Its shift by -0.75 V was interpreted by the authors of Ref. [362] as the respective change in the position of the Fermi level in SWCNTs.

Measurement of the work function of filled SWCNTs. The shift of the Fermi level can be directly determined by studying the spectra of secondary electrons, i.e., SWCNT electrons that received sufficient energy from photoelectrons to escape into the vacuum (in excess of the work function), measured by photoemission spectroscopy.

Some papers describe the secondary electron cutoff spectra of SWCNTs filled with copper [362] and zinc [368] halogenides as sharp peaks having the maxima in a kinetic

energy range from 4.5 to 5 eV. The authors defined the work function as the kinetic energy at half peak height. According to Ref. [362], it was equal to 4.6 eV for pristine SWCNTs, and 4.8, 5.2, and 5.25 eV for nanotubes filled with copper iodide, bromide, and chloride, respectively. The work function variation being directly related to changes in the Fermi level position, the data obtained were used to calculate the shift of the Fermi level for filled SWCNTs; it proved to be −0.2, −0.6, and −0.65 eV using CuI, CuBr, and CuCl molecules, respectively, as the encapsulating materials [362].

Ultraviolet photoelectron spectroscopy. UPS approach allows studying the modification of the nanotube valence band associated with their filling. The valence band spectrum has a shape typical of all allotropic carbon modifications with sp^2-hybridization; it is characterized by the presence of two main peaks, π- and σ-resonances. One of them is located at a binding energy of 3 eV and corresponds to photoelectron emission from the π-band of nanotubes, while the other lies at 8 eV and is related to photoelectron emission from the σ-band (Fig. 13a) [434]. High-resolution spectroscopic measurements for a high-purity SWCNT sample with narrow diameter distribution revealed three additional peaks on the low-binding energy side of π-resonance near the Fermi level, which correspond to individual SWCNT van Hove singularities [195, 435] (S_1, S_2 are the first and second singularities of semiconducting SWCNTs, respectively, and M_1 is the first van Hove singularity of metallic nanotubes in Fig. 13b).

Modification of valence band spectra (viz. a shift of π- and σ-resonances, as well as van Hove singularity peaks, changes in their intensity or disappearance, and variations of the density of electron states at the Fermi level) may indicate an alteration of SWCNT electronic properties. There are reports in the literature on recording the valence band spectra of nanotubes encapsulated with $Gd@C_{82}$ molecules [301], erbium chloride [359], copper [362] and zinc [368] halogenides, cerocene [331, 332], C_{60} molecules [288], ferrocene [324, 326, 328], and europium [358] (see Table 2).

In the case of nanotubes filled with $Ce(C_5H_5)_3$ [331, 332] or Eu [358] and samples obtained by thermal treatment of SWCNTs with previously encapsulated $Gd@C_{82}$ [301] or $ErCl_3$ [359] molecules, the authors observed a rise in the density of electron states at the Fermi level presumably due to charge transfer to the SWCNT walls. For nanotubes filled with copper [362] and zinc [368] halogenides, they found a shift of π-resonance toward lower binding energies and interpreted it as a result of a downward displacement of the nanotube Fermi level.

Modification of van Hove singularity peaks was studied for nanotubes filled with europium [358] and ferrocene [326, 328]. Figure 13b presents valence band spectra of pristine and Eu-filled nanotubes. In the latter case, the peaks were shifted into the high-energy region by 0.1 eV, which corresponded to a comparable elevation of the Fermi level, i.e., donor doping of SWCNTs, and agreed with a rise in the density of electron states at the Fermi level (Fig. 13b). The estimated number of transferred electrons was 1.79 per Eu atom [358].

Van Hove singularity peaks in the ultraviolet photoelectron spectrum of nanotubes filled with ferrocene molecules (Fig. 13c) were also shifted toward higher binding energies, which suggested charge transfer onto the SWCNT walls. Heating the sample resulted in ferrocene decomposition accompanied by a shift of van Hove singularity peaks in the opposite direction down to the values below those characteristic of pristine SWCNTs; in other words, donor doping changed to acceptor doping. The evaluated charge transfer density was $0.0067\,e^-$ Å^{-1} for ferrocene-filled SWCNTs, and $0.001\,e^-$ Å^{-1} for a sample annealed at 600 °C for 8 hours [326].

X-ray photoelectron spectroscopy. Investigations of C1s XPS spectra of filled nanotubes, corresponding to the emission of photoelectrons from the carbon core level, may provide information on the modification of SWCNT electronic structure. A change in the peak position, shape, or width may reflect an alteration of the electronic properties of SWCNTs. The authors of Ref. [429] undertook an analysis of C1s XPS spectra of pristine nanotubes with a mean diameter of 1.37 nm. The spectrum was shaped like a narrow peak with the maximum at an electron binding energy of 284.65 eV; its width at half height was 0.4 eV, slightly greater than the value of 0.32 eV for graphite due to the presence of nanotubes with a certain diameter distribution in the sample [429].

The literature describes results of studies on C1s spectra of nanotubes filled with $Gd@C_{82}$ molecules [301], ferrocene [324, 326], cerocene [331, 332], europium [358], erbium chloride [359], silver [361], copper [362], iron [369], nickel

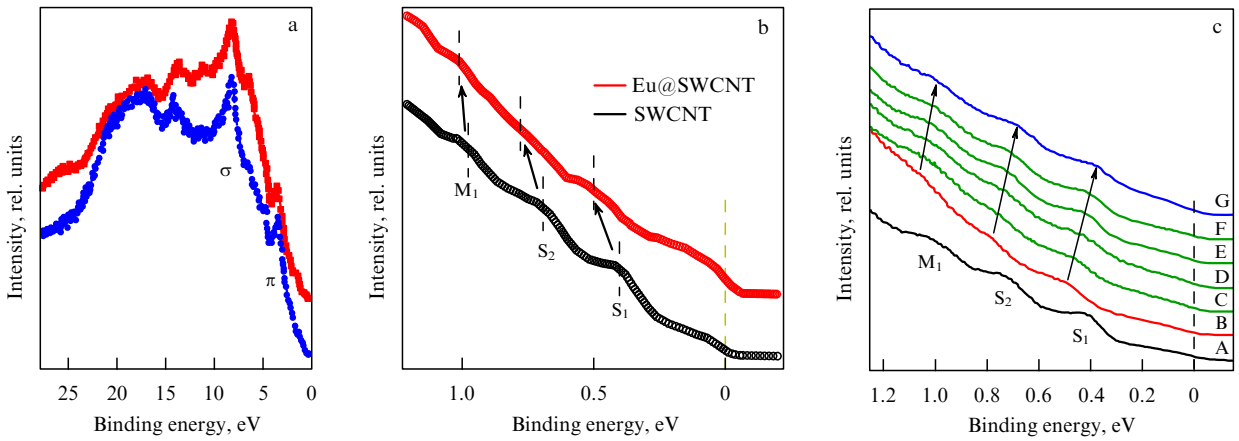

Figure 13. (Color online.) (a) Valence band spectra of SWCNTs with metallic (upper curve) and semiconducting (lower curve) conductivity [434], (b) UPS spectra of pristine and Eu-filled nanotubes [358], and (c) valence band spectra of pristine SWCNTs (A), ferrocene-filled nanotubes (B), and a sample (B) annealed in a vacuum at 600 °C for 2 h (C), 8 h (D), 54 h (E), and 212 h (F), and at 1150 °C for 1 hr (G) [326].

[366], manganese [367], and zinc [365, 368] halogenides, cobalt bromide [379], cadmium chloride [365], terbium chloride [365], tin telluride [397], silver [347, 348], and copper [347, 353] (see Table 2).

The authors of Refs [301, 324, 326, 331, 332, 358, 359] carried out qualitative analyses of the C1s peak; they related broadening of the spectrum, its increased asymmetry, and the shift of the maximum to a possible presence of charge transfer, which was confirmed by other methods as well. Individual components were distinguished in the spectra of SWCNTs encapsulated with silver [361], copper [362], iron [369], nickel [366], manganese [367], and zinc [365, 368] halogenides, cobalt bromide [379], cadmium chloride [365], terbium chloride [365], silver [347, 348], and copper [347, 353]. C1s XPS spectra of nanotubes filled with silver halogenides [361] were fitted by three components (Fig. 14a), one of which corresponded to pristine nanotubes (I in Fig. 14a), and the other two of which corresponded to filled ones (II and III, respectively, in Fig. 14a). The second component shifted by −0.38 eV with respect to the first one in AgCl, by −0.3 eV in AgBr, and by −0.30 eV in AgI appeared as a result of a change in the work function of nanotubes after encapsulation of silver halogenides due to the decreased Fermi energy and the respective shift of the spectral components of filled SWCNTs toward lower binding energies. Thus, the peak shift corresponded to the displacement of the Fermi level. The appearance of the third component was related to possible local interactions between the SWCNT wall and atoms of the doping compounds (Fig. 14a) [361].

The authors applied the same line of reasoning to the analysis of C1s spectra of SWCNTs filled with copper halogenides [362]. However, higher-resolution studies of the spectra made it possible to distinguish components corresponding to metallic and semiconducting nanotubes. Indeed, it was shown in Ref. [429] that the C1s peak of SWCNTs unsorted by conductivity type may contain components of metallic and semiconducting nanotubes with the maxima positioned at binding energies of 284.60 and 284.70 eV, respectively, and the widths at half height equal to 0.31 and 0.39 eV. The shift of the metallic nanotube component by 0.1 eV toward lower binding energies was attributed to the difference in the work functions between SWCNTs with different types of conduction. In a later study [434], C1s XPS spectra of nanotubes sorted by conduction type were recorded. Peak maxima of metallic and semiconducting SWCNTs were found to lie at 284.43 and 284.48 eV, while their high-height widths equaled 0.26 and 0.32 eV, respectively (Fig. 14b). The peak of metallic nanotubes was characterized by the asymmetry parameter $\alpha = 0.11$ [434].

Bearing in mind the above differences between C1s XPS spectra of nanotubes with different types of conductivity, the authors of Ref. [362] fitted the spectra of SWCNTs filled with copper halogenides with five components. Figure 14c presents C1s spectra of SWCNTs filled with copper bromide and fitted with five components of pristine metallic and semiconducting nanotubes (I and II, respectively, in Fig. 14c), filled SWCNTs possessing metallic and semiconducting conductivity (IV and V, respectively, in Fig. 14c), and a component corresponding to local interactions between the SWCNT wall atoms and the encapsulated copper bromide (VI in Fig. 14c) [362]. The shifts of the components of the filled metallic and semiconducting SWCNTs relative to those of the pristine ones were −0.57 and −0.375 eV, respectively, for CuCl, −0.60 and −0.365 eV for CuBr, and −0.35 and −0.255 eV for CuI.

5.2 Simulation of the electronic properties of filled SWCNTs

Investigations of the electronic properties of filled nanotubes by experimental methods can be supplemented by quantum-chemical simulations. Literature publications report on basic research concerning the simulation of the band structure of filled nanotubes with different chiral vectors, their density of electron states, the dependence of the electronic properties on nanotube diameter, and the correlation between the structure of doping compounds and their influence on the electronic properties of SWCNTs.

Simulation of electronic properties of filled SWCNTs was first reported by Russian researchers in 1993 [436]. They calculated the band structure of filled $[Li@C_{24}]_n$ and $[K@C_{36}]_n$ nanotubes in which charge transfer from the SWCNT walls to encapsulated metal atoms was observed. Later on, the electronic properties of armchair and zigzag nanotubes filled with C_{60} [437–442], C_{70}, C_{78}, and C_{82} [439–441] molecules, and $La@C_{82}$, $K@C_{60}$, $Ca@C_{60}$, and $Y@C_{60}$ endofullerenes [437–439] were also investigated (see Table 2). It was shown that the influence of C_{60} fullerenes on the electronic properties of SWCNTs depends on their diameter. Encapsulation of molecules into SWCNTs more than 1.18 nm in diameter results in a nanostructure with a small charge transfer from the tube walls, whereas filling SWCNTs less than 1.18 nm in diameter leads to a detectable charge transfer from the C_{60} molecules to the nanotube walls [442]. As shown

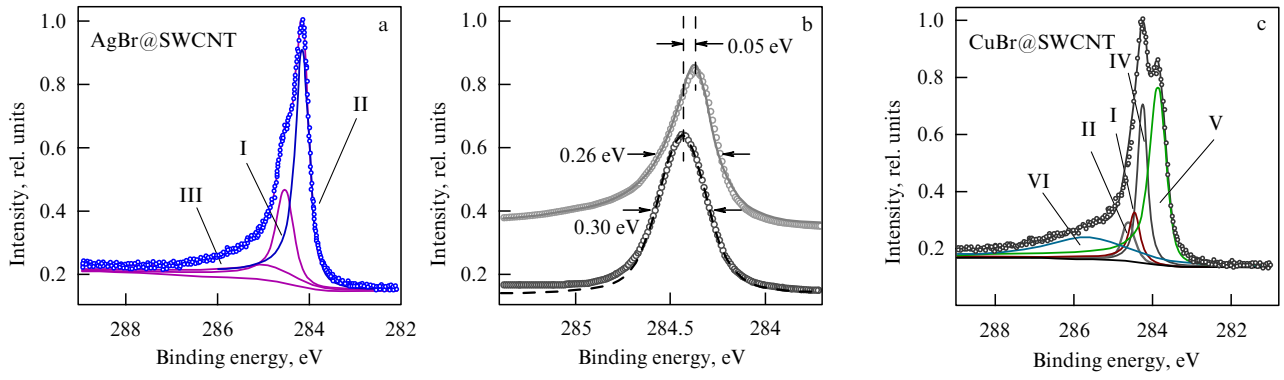

Figure 14. (Color online.) C1s XPS spectra of silver bromide-filled nanotubes (a) [361], pristine metallic (upper curve) and semiconducting (lower curve) SWCNTs (b) [434], and copper bromide-filled nanotubes (c) [362].

in Ref. [437], the effectiveness of charge transfer from the SWCNT walls to the doping agents in the case of endohedral K@C_{60}, Ca@C_{60}, and Y@C_{60} fullerenes is higher than for C_{60} molecules.

The authors of Ref. [443] demonstrated that the encapsulation of electrophilic organic molecules (TCNQ and F_4TCNQ) into SWCNT channels results in acceptor doping of nanotubes, whereas the insertion of nucleophilic organic (TTF and TDAE) and metallo-organic (cobaltocene) molecules causes donor doping of nanotubes. The donor influence of other metallocenes on SWCNT electronic properties was studied in Refs [326, 444, 445] for $M(C_5H_5)_2$ compounds, where M = V, Cr, Mn, Fe, Co, and Ni.

Moreover, the literature contains reports on donor doping of SWCNTs by encapsulating such metals as Ti, Zn [446], Co, Ni [447], Fe [446, 448, 449], Mo [450], Gd [451, 452], Eu [451], Cu [453], and Ag [454, 455] (see Table 2). Calculations of the band structure of filled (8, 0) nanotubes in Ref. [454] allowed the influence of Ag and CrO_3 on their electronic properties to be compared. Figure 15 depicts the band structures thus obtained, suggesting that silver exerts a donor effect apparent from the appearance of the half-occupied level in the SWCNT band gap (Fig. 15b), whereas CrO_3 has an acceptor effect (Fig. 15c). These data agree with the experimental findings described in paper [350].

There are also publications on the simulation of electronic properties of SWCNTs filled with potassium iodide [456], incorporation of which was accompanied by a very small charge transfer from the nanotube wall to the nanocrystal. Mercury telluride was also used as a filling agent [394, 395] with the result that the electronic properties of one-dimensional HgTe nanocrystals were drastically different from those of three-dimensional crystals. Calculations showed that a 1D crystal of HgTe is a semiconductor with a $\sim$ 1.2-eV bandgap, whereas a 3D crystal exhibits semimetallic properties.

6. Applications of filled SWCNTs

The possibility of encapsulating substances with a wide range of chemical and physical properties into SWCNT channels opens up good prospects for the use of resulting nanostructures in various fields. Filled SWCNTs may find application in nanoelectronic devices, for the fabrication of electrodes for supercapacitors, and as catalytic agents, sensors, and auto-electron emitters. Also, they may be employed for processing quantum information, for targeted drug delivery, or as radiographic markers in the course of studying living organisms (Fig. 16).

The use of filled nanotubes in *nanoelectronic devices* is a most promising application of these nanostructures [273, 287, 296, 307, 311, 413, 414, 457–466]. By way of example, it was shown that SWCNTs filled with C_{60} fullerenes can serve as channels of p-type field-effect transistors [465]. Simultaneously, the studies reported in papers [460, 463, 465] demonstrated that nanotube channel filling with Gd@C_{82} endofullerene narrows the bandgap of SWCNTs from $\sim$ 0.5 to $\sim$ 0.1 eV, which enables such nanostructures to be utilized as channels in transistors with ambipolar conduction.

References [296, 457] first reported the temperature dependence of conduction in SWCNTs filled with Dy@C_{82} endofullerenes. Specifically, such structures behaved as p-type materials at room temperature but exhibited n-type conduction when the temperature dropped to 265 K. High-temperature superconductivity of fullerene-filled SWCNTs was predicted in Ref. [464].

Moreover, some authors have suggested using filled SWCNTs for designing high-performance nanoelectronic circuits [408]. Reference [461] described the design of an air-stable p–n transition based on partially filling the SWCNT channel with iron. The authors of a later study [408] managed for the first time to realize an air-stable p–n transition by means of the simultaneous filling of the SWCNT channel with

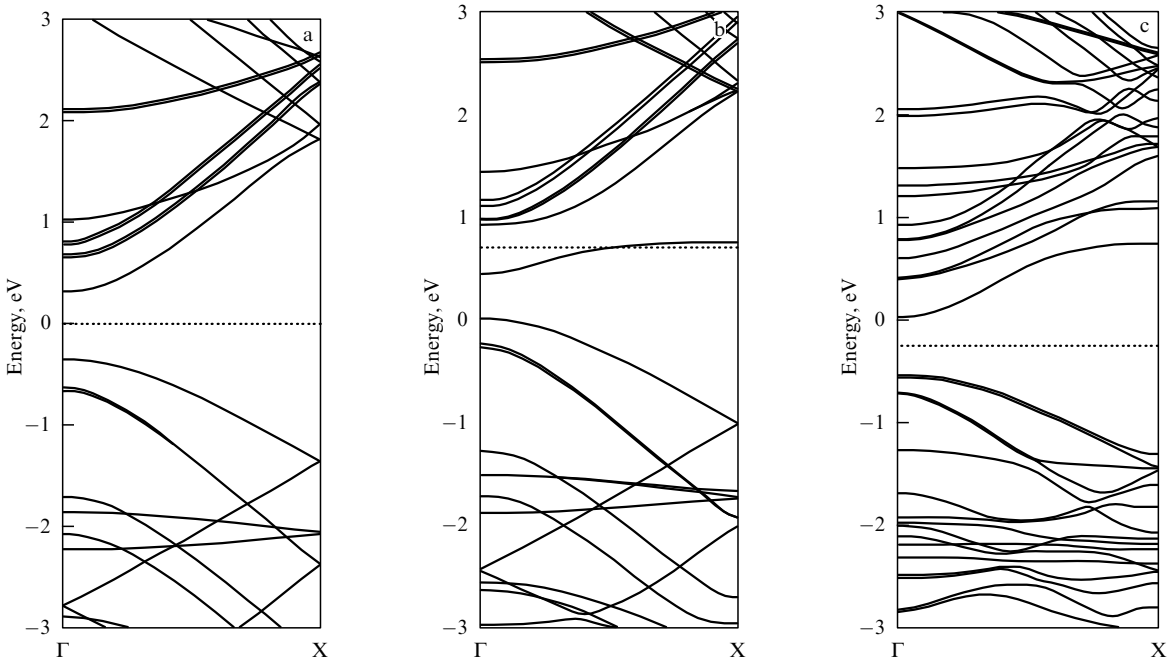

Figure 15. Band structures of pristine (8, 0) nanotubes (a), SWCNTs filled with silver (b) and chromium oxide (CrO_3) (c) [454]. The dotted line marks the position of the Fermi level.

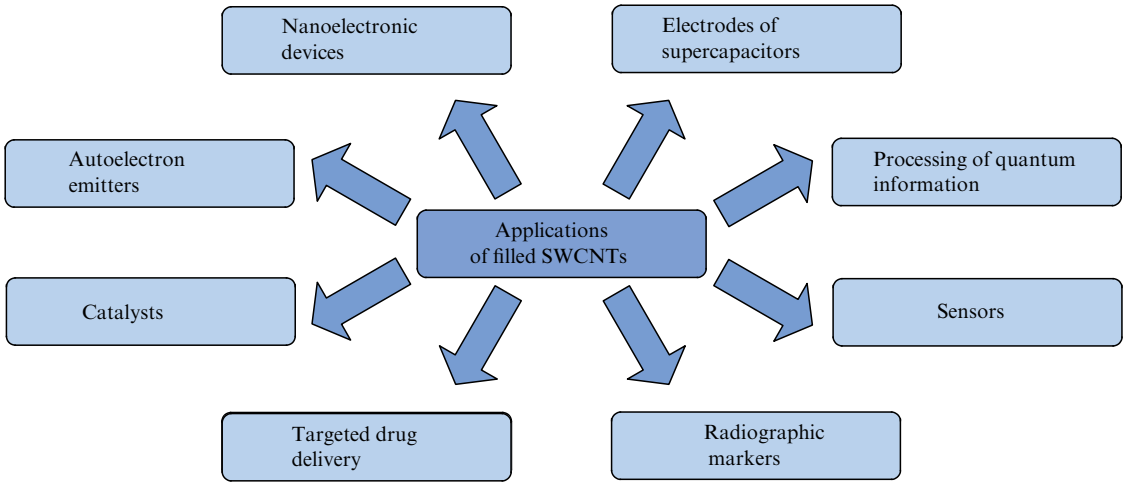

Figure 16. Diagram illustrating potential applications of filled SWCNTs.

electron donors and acceptors (caesium and iodine, as well as Cs atoms and C_{60} molecules). It turned out that the transport properties of SWCNTs are directly related to the doping level and can be controlled in the course of filling the nanotube channels [273].

One of the possible applications of such nanostructures is the fabrication of electrodes for supercapacitors. As shown in Ref. [467], the use of chromium oxide (CrO_3)-filled nanotubes as a material for the electrodes of symmetric supercapacitors makes it possible to achieve an extremely high-rate charging.

The authors of Ref. [354] suggested that clusters of transition metals distributed in the internal channels of SWCNTs may be suitable for *catalytic applications*, because nanoparticles having a smaller diameter show higher catalytic activity and influence the rate of chemical reactions. As noted in Ref. [415], if SWCNTs filled with catalytic nanoparticles are mixed up with the components of a chemical process, the graphene wall will prevent contact between mixture constituents. Under specific conditions, the wall of the nanotube breaks down, and the catalyst becomes activated.

It was shown in Ref. [468] that SWCNTs filled with copper iodide are characterized by a low electron work function, which makes it possible to employ such nanostructures in fabricating *autoelectron emitters* for modern electroluminescent tubes and X-ray minitubes [414].

It was speculated that SWCNTs filled with fullerenes containing specific functional groups may find application in designing *sensors* [315]. Moreover, the authors of Ref. [469] demonstrated that fullerene-filled SWCNTs may be useful for *processing quantum information* and creating a quantum computer.

Finally, filled SWCNTs may also find application in medicine, e.g., for *targeted drug delivery*. Medications can be chemically attached to fullerenes encapsulated into SWCNT channels and delivered directly to the affected organs, tissues, or cells (in such cases, a nanotube serves as a nanosyringe) [415]. One more application of nanotubes containing endohedral fullerenes with encapsulated atoms of radioactive elements centers around their use as *markers* in radiographic studies of living organisms [415].

7. Conclusion

Breakthrough research over the past 5 years has greatly contributed to the understanding of the effects exerted by the materials encapsulated into channels of SWCNTs on their electronic properties. The employment of various spectroscopic techniques, such as Raman spectroscopy, X-ray photoelectron spectroscopy, optical absorption spectroscopy, X-ray emission spectroscopy, X-ray absorption spectroscopy, UV photoelectron spectroscopy, and photoluminescence spectroscopy, have made possible precision studies on the modification of the electronic properties of nanotubes filled with different substances at the qualitative and quantitative levels.

The present review is focused on current status of research on the electronic properties of filled SWCNTs. Special attention is given to atomic structure and its relationship with the electronic properties. Methods for the modification of SWCNT electronic properties are described, including chemical modification of the outer surface of single-walled carbon nanotubes with the use of functional groups and molecules forming no chemical bonds, the substitution of carbon atoms in the nanotube walls by other atoms, the intercalation of nanotube bundles, electrochemical doping, and filling of nanotube channels. SWCNT-filling materials are organized into a system. The literature data concerning experimental investigations of electronic properties of filled nanotubes are summarized and analyzed both qualitatively (detection of charge transfer and its direction) and quantitatively (measurement of electron work function, determination of the Fermi level and its shift relative to the initial position). Furthermore, the results of theoretical research are summarized, with an emphasis on the quantum-chemical simulation of the electronic properties of filled SWCNTs. Possible application areas of filled SWCNTs are described.

The author hopes that this review will be useful and interesting to a wide circle of researchers and promote further progress in studies of filled single-walled carbon nanotubes.

References

1. Hughes T V, Chambers C R, US Patent 405,480 (1889)
2. Edison T A, US Patent 470,925 (1892)
3. Radushkevich L V, Luk'yanovich V M *Zh. Fiz. Khim.* **26** 88 (1952)
4. Oberlin A, Endo M, Koyama T *J. Cryst. Growth* **32** 335 (1976)
5. Oberlin A, Endo M, Koyama T *Carbon* **14** 133 (1976)
6. Iijima S *Nature* **354** 56 (1991)
7. Kosakovskaya Z Ya, Chernozatonskii L A, Fedorov E A *JETP Lett.* **56** 26 (1992) [*Pis'ma Zh. Eksp. Teor. Fiz.* **56** 26 (1992)]
8. Bethune D S et al. *Nature* **363** 605 (1993)
9. Iijima S, Ichihashi T *Nature* **363** 603 (1993)
10. Ajayan P M, Iijima S *Nature* **361** 333 (1993)
11. Seraphin S et al. *Nature* **362** 503 (1993)
12. Ajayan P M et al. *Nature* **362** 522 (1993)
13. Saito Y, Yoshikawa T *J. Cryst. Growth* **134** 154 (1993)
14. Smith B W, Monthioux M, Luzzi D E *Nature* **396** 323 (1998)
15. Sloan J et al. *Chem. Commun.* (3) 347 (1998)
16. Balasubramanian K, Burghard M *Small* **1** 180 (2005)
17. Saito R, Dresselhaus G, Dresselhaus M S *Physical Properties of Carbon Nanotubes* (London: Imperial College Press, 1998)
18. Charlier J-C, Blase X, Roche S *Rev. Mod. Phys.* **79** 677 (2007)
19. Hertel T, Walkup R E, Avouris P *Phys. Rev. B* **58** 13870 (1998)
20. Dervishi E et al. *Particulate Sci. Technol.* **27** 107 (2009)
21. Fuhrer M S, in *Advanced Semiconductor and Organic Nano-Techniques* Vol. 2 (Ed. H Morkoç) (Amsterdam: Elsevier Science, 2003) p. 293
22. Kreupl F, in *Carbon Nanotube Devices* (Advanced Micro & Nanosystems, Vol. 8, Ed. C Hierold) (Weinheim: Wiley-VCH, 2008) p. 1
23. Painter G S, Ellis D E *Phys. Rev. B* **1** 4747 (1970)
24. Saito R, Kataura H, in *Carbon Nanotubes* (Topics in Applied Physics, Vol. 80, Eds M S Dresselhaus, G Dresselhaus, P Avouris) (Berlin: Springer, 2001) p. 213
25. Wallace P R *Phys. Rev.* **71** 622 (1947)
26. Mintmire J W, Dunlap B I, White C T *Phys. Rev. Lett.* **68** 631 (1992)
27. Dresselhaus M S, Dresselhaus G, Saito R *Carbon* **33** 883 (1995)
28. Saito R et al. *Appl. Phys. Lett.* **60** 2204 (1992)
29. Kim P et al. *Phys. Rev. Lett.* **82** 1225 (1999)
30. Odom T W et al. *Nature* **391** 62 (1998)
31. Odom T W et al. *J. Mater. Res.* **13** 2380 (1998)
32. Wilder J W G et al. *Nature* **391** 59 (1998)
33. Ajiki H, Ando T *Physica B* **201** 349 (1994)
34. Kataura H et al. *AIP Conf. Proc.* **486** 328 (1999)
35. Kazaoui S et al. *Phys. Rev. B* **60** 13339 (1999)
36. Alvarez L et al. *Chem. Phys. Lett.* **316** 186 (2000)
37. Kasuya A et al. *Phys. Rev. Lett.* **78** 4434 (1997)
38. Pimenta M A et al. *J. Mater. Res.* **13** 2396 (1998)
39. Pimenta M A et al. *Phys. Rev. B* **58** R16016 (1998)
40. Rao A M et al. *Science* **275** 187 (1997)
41. Charlier J-C, Lambin Ph *Phys. Rev. B* **57** R15037 (1998)
42. Mintmire J W, White C T *Phys. Rev. Lett.* **81** 2506 (1998)
43. White C T, Todorov T N *Nature* **393** 240 (1998)
44. Kataura H et al. *Synthet. Met.* **103** 2555 (1999)
45. Kane C L, Mele E J *Phys. Rev. Lett.* **78** 1932 (1997)
46. Delaney P et al. *Nature* **391** 466 (1998)
47. Ouyang M et al. *Science* **292** 702 (2001)
48. Charlier J-C, Gonze X, Michenaud J-P *Europhys. Lett.* **29** 43 (1995)
49. Reich S, Thomsen C, Ordejón P *Phys. Rev. B* **65** 155411 (2002)
50. Fan Y W, Goldsmith B R, Collins P G *Nature Mater.* **4** 906 (2005)
51. Hashimoto A et al. *Nature* **430** 870 (2004)
52. Gómez-Navarro C et al. *Nature Mater.* **4** 534 (2005)
53. Charlier J-C, Ebbesen T W, Lambin Ph *Phys. Rev. B* **53** 11108 (1996)
54. Chico L et al. *Phys. Rev. Lett.* **76** 971 (1996)
55. Dunlap B I *Phys. Rev. B* **49** 5643 (1994)
56. Lambin Ph et al. *Chem. Phys. Lett.* **245** 85 (1995)
57. Saito R, Dresselhaus G, Dresselhaus M S *Phys. Rev. B* **53** 2044 (1996)
58. Ouyang M et al. *Science* **291** 97 (2001)
59. Yao Z et al. *Nature* **402** 273 (1999)
60. Tasis D et al. *Chem. Rev.* **106** 1105 (2006)
61. Monthioux M, Flahaut E, Cleuziou J-P *J. Mater. Res.* **21** 2774 (2006)
62. Andrews R et al. *Acc. Chem. Res.* **35** 1008 (2002)
63. Bahr J L, Tour J M *J. Mater. Chem.* **12** 1952 (2002)
64. Banerjee S, Kahn M G C, Wong S S *Chemistry A Eur. J.* **9** 1898 (2003)
65. Banerjee S, Hemraj-Benny T, Wong S S *Adv. Mater.* **17** 17 (2005)
66. Dai L, Mau A W H *Adv. Mater.* **13** 899 (2001)
67. Davis J J et al. *Chemistry A Eur. J.* **9** 3732 (2003)
68. de la Torre G, Blau W, Torres T *Nanotechnology* **14** 765 (2003)
69. Dyke C A, Tour J M *J. Phys. Chem. A* **108** 11151 (2004)
70. Dyke C A, Tour J M *Chemistry A Eur. J.* **10** 812 (2004)
71. Fischer J E *Acc. Chem. Res.* **35** 1079 (2002)
72. Fu K, Sun Y-P *J. Nanosci. Nanotechnol.* **3** 351 (2003)
73. Hilding J et al. *J. Dispers. Sci. Technol.* **24** 1 (2003)
74. Hirsch A *Angew. Chem. Int. Ed.* **41** 1853 (2002)
75. Hirsch A, Vostrowsky O, in *Functional Molecular Nanostructures* (Topics in Current Chemistry, Vol. 245, Ed. A D Schluter) (Berlin: Springer, 2005) p. 193
76. Katz E, Willner I *ChemPhysChem* **5** 1084 (2004)
77. Lin T et al. *Australian J. Chem.* **56** 635 (2003)
78. Lu X, Chen Z *Chem. Rev.* **105** 3643 (2005)
79. Niyogi S et al. *Acc. Chem. Res.* **35** 1105 (2002)
80. Rao C N R et al. *ChemPhysChem* **2** 78 (2001)
81. Sinnott S B *J. Nanosci. Nanotechnol.* **2** 113 (2002)
82. Sun Y-P et al. *Acc. Chem. Res.* **35** 1096 (2002)
83. Tasis D et al. *Chemistry A Eur. J.* **9** 4000 (2003)
84. Terrones M *Annu. Rev. Mater. Res.* **33** 419 (2003)
85. Thostenson E T, Ren Z, Chou T-W *Composit. Sci. Technol.* **61** 1899 (2001)
86. Hamwi A et al. *Carbon* **35** 723 (1997)
87. Kawasaki S et al. *Phys. Chem. Chem. Phys.* **6** 1769 (2004)
88. Mickelson E T et al. *Chem. Phys. Lett.* **296** 188 (1998)
89. Nakajima T, Kasamatsu S, Matsuo Y *Eur. J. Solid State Inorg. Chem.* **33** 831 (1996)
90. Touhara H, Okino F *Carbon* **38** 241 (2000)
91. Touhara H et al. *J. Fluorine Chem.* **114** 181 (2002)
92. Yudanov N F et al. *Chem. Mater.* **14** 1472 (2002)
93. Kelly K F et al. *Chem. Phys. Lett.* **313** 445 (1999)
94. An K H et al. *Appl. Phys. Lett.* **80** 4235 (2002)
95. Brzhezinskaya M M et al. *Fullerenes Nanotubes Carbon Nanostruct.* **18** 590 (2010)
96. Lee Y S et al. *J. Fluorine Chem.* **120** 99 (2003)
97. Plank N O V, Jiang L, Cheung R *Appl. Phys. Lett.* **83** 2426 (2003)
98. Plank N O V, Cheung R *Microelectron. Eng.* **73–74** 578 (2004)
99. Fedoseeva Yu V et al. *Fullerenes Nanotubes Carbon Nanostruct.* **18** 595 (2010)
100. Bettinger H F, Kudin K N, Scuseria G E *J. Am. Chem. Soc.* **123** 12849 (2001)
101. Bettinger H F *ChemPhysChem* **4** 1283 (2003)
102. Bettinger H F *Org. Lett.* **6** 731 (2004)
103. Jaffe R L *J. Phys. Chem. B* **107** 10378 (2003)
104. Kudin K N, Bettinger H F, Scuseria G E *Phys. Rev. B* **63** 045413 (2001)
105. Lebedev N G, Zaporotskova I V, Chernozatonskii L A *Microelectron. Eng.* **69** 511 (2003)
106. Root M J *Nano Lett.* **2** 541 (2002)
107. Van Lier G et al. *J. Phys. Chem. B* **109** 6153 (2005)
108. Pehrsson P E et al. *J. Phys. Chem. B* **107** 5690 (2003)
109. Zhao W et al. *J. Phys. Chem. B* **106** 293 (2002)
110. Coleman K S et al. *Chem. Mater.* **19** 1076 (2007)
111. Alvaro M et al. *J. Phys. Chem. B* **108** 12691 (2004)
112. Callegari A et al. *Chem. Commun.* 2576 (2003)
113. Chen J et al. *Science* **282** 95 (1998)
114. Georgakilas V et al. *J. Am. Chem. Soc.* **124** 760 (2002)
115. Guldi D M et al. *Angew. Chem. Int. Ed.* **42** 4206 (2003)
116. Wang Y, Iqbal Z, Mitra S *Carbon* **43** 1015 (2005)
117. Bahr J L et al. *J. Am. Chem. Soc.* **123** 6536 (2001)
118. Dyke C A, Tour J M *Nano Lett.* **3** 1215 (2003)
119. Dyke C A et al. *Synlett* 155 (2004)
120. Leventis H C et al. *ChemPhysChem* **6** 590 (2005)
121. Marcoux P R et al. *New J. Chem.* **28** 302 (2004)
122. Strano M S et al. *Science* **301** 1519 (2003)
123. Strano M S *J. Am. Chem. Soc.* **125** 16148 (2003)
124. Shiral Fernando K A et al. *J. Am. Chem. Soc.* **126** 10234 (2004)

125. Fifield L S et al. *J. Phys. Chem. B* **108** 8737 (2004)
126. Nakashima N, Tomonari Y, Murakami H *Chem. Lett*. **31** 638 (2002)
127. Paloniemi H et al. *J. Phys. Chem. B* **109** 8634 (2005)
128. Zhang J et al. *Nano Lett*. **3** 403 (2003)
129. Islam M F et al. *Nano Lett*. **3** 269 (2003)
130. Matarredona O et al. *J. Phys. Chem. B* **107** 13357 (2003)
131. Moore V C et al. *Nano Lett*. **3** 1379 (2003)
132. Lee J-H et al. *J. Phys. Chem. C* **111** 2477 (2007)
133. Geng H-Z et al. *J. Am. Chem. Soc*. **129** 7758 (2007)
134. Kim K K et al. *Adv. Funct. Mater*. **17** 1775 (2007)
135. Shin H-J et al. *J. Am. Chem. Soc*. **130** 2062 (2008)
136. Collins P G et al. *Science* **287** 1801 (2000)
137. Kong J et al. *Science* **287** 622 (2000)
138. Ayala P et al. *Rev. Mod. Phys*. **82** 1843 (2010)
139. Yi J-Y, Bernholc J *Phys. Rev. B* **47** 1708 (1993)
140. Ayala P et al. *J. Phys. Chem. C* **111** 2879 (2007)
141. Elías A L et al. *J. Nanosci. Nanotechnol*. **10** 3959 (2010)
142. Glerup M et al. *Chem. Phys. Lett*. **387** 193 (2004)
143. Keskar G et al. *Chem. Phys. Lett*. **412** 269 (2005)
144. Krstić V et al. *Europhys. Lett*. **77** 37001 (2007)
145. Lin H et al. *Phys. Status Solidi B* **245** 1986 (2008)
146. Lin H et al. *J. Phys. Chem. C* **113** 9509 (2009)
147. Maciel I O et al. *Nature Mater*. **7** 878 (2008)
148. Susi T et al. *Phys. Status Solidi B* **247** 2726 (2010)
149. Villalpando-Paez F et al. *Chem. Phys. Lett*. **424** 345 (2006)
150. Wiltshire J G et al. *Phys. Rev. B* **72** 205431 (2005)
151. Ayala P et al. *J. Mater. Chem*. **18** 5676 (2008)
152. Ayala P et al. *Appl. Phys. Lett*. **96** 183110 (2010)
153. Borowiak-Palen E et al. *Chem. Phys. Lett*. **378** 516 (2003)
154. Borowiak-Palen E et al. *Carbon* **42** 1123 (2004)
155. Daothong S et al. *Phys. Status Solidi B* **246** 2518 (2009)
156. Fuentes G G et al. *Phys. Rev. B* **69** 245403 (2004)
157. Gai P L et al. *J. Mater. Chem*. **14** 669 (2004)
158. McGuire K et al. *Carbon* **43** 219 (2005)
159. Ayala P et al. *Carbon* **48** 575 (2010)
160. Kang H S, Jeong S *Phys. Rev. B* **70** 233411 (2004)
161. Nevidomskyy A H, Csányi G, Payne M C *Phys. Rev. Lett*. **91** 105502 (2003)
162. Terrones M, Souza A G, Rao A M, in *Carbon Nanotubes* (Topics in Applied Physics, Vol. 111, Eds A Jorio, G Dresselhaus, M S Dresselhaus) (Berlin: Springer, 2008) p. 531
163. Czerw R et al. *Nano Lett*. **1** 457 (2001)
164. Rocha A R et al. *Phys. Rev. B* **77** 153406 (2008)
165. Wirtz L, Rubio A *AIP Conf. Proc*. **685** 402 (2003)
166. Gracia J, Kroll P *J. Mater. Chem*. **19** 3020 (2009)
167. Baierle R J et al. *Phys. Rev. B* **64** 085413 (2001)
168. Fagan S B et al. *Mater. Characterization* **50** 183 (2003)
169. Maciel I O et al. *Nano Lett*. **9** 2267 (2009)
170. Dresselhaus M S, Dresselhaus G *Adv. Phys*. **30** 139 (1981)
171. Dresselhaus M S, Dresselhaus G, Eklund P C *Science of Fullerenes and Carbon Nanotubes* (San Diego: Academic Press, 1996)
172. Rao A M et al. *Nature* **388** 257 (1997)
173. Lee R S et al. *Nature* **388** 255 (1997)
174. Bandow S et al. *Appl. Phys. A* **71** 561 (2000)
175. Baxendale M et al. *Phys. Rev. B* **56** 2161 (1997)
176. Bockrath M et al. *Phys. Rev. B* **61** R10606 (2000)
177. Bower C et al. *Appl. Phys. A* **67** 47 (1998)
178. Claye A, Fischer J E *Mol. Cryst. Liq. Cryst*. **340** 743 (2000)
179. Duclaux L et al. *Mol. Cryst. Liq. Cryst*. **340** 769 (2000)
180. Duclaux L *Carbon* **40** 1751 (2002)
181. Duclaux L et al. *J. Phys. Chem. Solids* **64** 571 (2003)
182. Galambos M et al. *Phys. Status Solidi B* **246** 2760 (2009)
183. Jouguelet E, Mathis C, Petit P *Chem. Phys. Lett*. **318** 561 (2000)
184. Kramberger C et al. *Phys. Rev. B* **79** 195442 (2009)
185. Kramberger C et al. *Phys. Status Solidi B* **246** 2693 (2009)
186. Kukovecz A et al. *Phys. Chem. Chem. Phys*. **5** 582 (2003)
187. Lee R S et al. *Phys. Rev. B* **61** 4526 (2000)
188. Liu X et al. *Phys. Rev. B* **67** 125403 (2003)
189. Liu X et al. *Phys. Rev. B* **70** 245435 (2004)
190. Petit P et al. *Chem. Phys. Lett*. **305** 370 (1999)
191. Pichler T et al. *Solid State Commun*. **109** 721 (1999)
192. Pichler T et al. *Synthet. Met*. **135 – 136** 717 (2003)
193. Pichler T et al. *New J. Phys*. **5** 156 (2003)
194. Pichler T et al. *Synthet. Met*. **153** 333 (2005)
195. Rauf H et al. *Phys. Rev. Lett*. **93** 096805 (2004)
196. Shimoda H et al. *Phys. Rev. Lett*. **88** 015502 (2002)
197. Simon F et al. *Phys. Status Solidi B* **245** 1975 (2008)
198. Suzuki S, Bower C, Zhou O *Chem. Phys. Lett*. **285** 230 (1998)
199. Suzuki S et al. *Appl. Phys. Lett*. **76** 4007 (2000)
200. Suzuki S et al. *Phys. Rev. B* **67** 115418 (2003)
201. Bower C et al. *Chem. Phys. Lett*. **288** 481 (1998)
202. De Blauwe K et al. *Phys. Status Solidi B* **246** 2732 (2009)
203. Fan X et al. *Phys. Rev. Lett*. **84** 4621 (2000)
204. Graupner R et al. *Phys. Chem. Chem. Phys*. **5** 5472 (2003)
205. Grigorian L et al. *Phys. Rev. Lett*. **80** 5560 (1998)
206. Hennrich F et al. *Phys. Chem. Chem. Phys*. **5** 178 (2003)
207. Kim K K et al. *J. Am. Chem. Soc*. **130** 12757 (2008)
208. Lee I H et al. *J. Phys. Chem. C* **114** 11618 (2010)
209. Liu X et al. *Phys. Rev. B* **70** 205405 (2004)
210. Sumanasekera G U et al. *J. Phys. Chem. B* **103** 4292 (1999)
211. Yoon S-M et al. *ACS Nano* **5** 1353 (2011)
212. Yu Z, Brus L E *J. Phys. Chem. A* **104** 10995 (2000)
213. Kukovecz A et al. *Chem. Commun*. 1730 (2002)
214. Fischer J E et al. *Phys. Rev. B* **31** 4773 (1985)
215. Zhou O et al. *Nature* **351** 462 (1991)
216. Monthioux M et al. *Carbon* **39** 1251 (2001)
217. Itkis M E et al. *Nano Lett*. **2** 155 (2002)
218. Bendiab N et al. *Phys. Rev. B* **64** 245424 (2001)
219. Iwasa Y et al. *Synthet. Met*. **121** 1203 (2001)
220. Rao A M et al. *Thin Solid Films* **331** 141 (1998)
221. Jacquemin R et al. *Synthet. Met*. **115** 283 (2000)
222. Ruzicka B et al. *Phys. Rev. B* **61** R2468 (2000)
223. Pichler T *New Diamond Frontier Carbon Technol*. **11** 375 (2001)
224. Bandow S et al. *Mol. Cryst. Liq. Cryst*. **340** 749 (2000)
225. Claye A S et al. *Phys. Rev. B* **62** R4845 (2000)
226. Grigorian L et al. *Phys. Rev. B* **58** R4195 (1998)
227. Kavan L, Dunsch L, in *Carbon Nanotubes* (Topics in Applied Physics, Vol. 111, Eds A Jorio, G Dresselhaus, M S Dresselhaus) (Berlin: Springer, 2008) p. 567
228. Cronin S B et al. *Appl. Phys. Lett*. **84** 2052 (2004)
229. Liu C-Y et al. *Electrochem. Solid-State Lett*. **2** 577 (1999)
230. Frackowiak E, Béguin F *Carbon* **39** 937 (2001)
231. Frackowiak E, Beguin F *Carbon* **40** 1775 (2002)
232. Heller I et al. *Nano Lett*. **5** 137 (2005)
233. Kavan L, Rapta P, Dunsch L *Chem. Phys. Lett*. **328** 363 (2000)
234. Kavan L et al. *J. Phys. Chem. B* **105** 10764 (2001)
235. An C P et al. *Synthet. Met*. **116** 411 (2001)
236. Corio P et al. *Chem. Phys. Lett*. **370** 675 (2003)
237. Corio P et al. *Chem. Phys. Lett*. **392** 396 (2004)
238. Ghosh S, Sood A K, Rao C N R *J. Appl. Phys*. **92** 1165 (2002)
239. Gupta S et al. *J. Appl. Phys*. **95** 2038 (2004)
240. Gupta S, Robertson J *J. Appl. Phys*. **100** 083711 (2006)
241. Gupta S *Diamond Relat. Mater*. **15** 378 (2006)
242. Kalbac M et al. *Phys. Status Solidi B* **243** 3134 (2006)
243. Kavan L, Dunsch L *Nano Lett*. **3** 969 (2003)
244. Kavan L, Dunsch L *ChemPhysChem* **4** 944 (2003)
245. Kavan L et al. *J. Phys. Chem. B* **109** 19613 (2005)
246. Kavan L et al. *Phys. Status Solidi B* **243** 3130 (2006)
247. Kazaoui S et al. *Synthet. Met*. **121** 1201 (2001)
248. Kazaoui S et al. *Appl. Phys. Lett*. **78** 3433 (2001)
249. Murakoshi K, Okazaki K *Electrochim. Acta* **50** 3069 (2005)
250. Okazaki K, Nakato Y, Murakoshi K *Phys. Rev. B* **68** 035434 (2003)
251. Okazaki K, Nakato Y, Murakoshi K *Surf. Sci*. **566** 436 (2004)
252. Rafailov P M et al. *Phys. Rev. B* **72** 045411 (2005)
253. Rafailov P M, Thomsen C *J. Optoelectron. Adv. Mater*. **7** 461 (2005)
254. Stoll M et al. *Chem. Phys. Lett*. **375** 625 (2003)
255. Wang Z et al. *Phys. Rev. Lett*. **96** 047403 (2006)
256. Kavan L, Dunsch L *ChemPhysChem* **8** 974 (2007)
257. Claye A et al. *Chem. Phys. Lett*. **333** 16 (2001)
258. Balasubramanian K, Burghard M *Analyt. Bioanalyt. Chem*. **385** 452 (2006)
259. Gong K et al. *Analytical Sciences* **21** 1383 (2005)
260. Gooding J J *Electrochim. Acta* **50** 3049 (2005)
261. Sherigara B S, Kutner W, D'Souza F *Electroanalysis* **15** 753 (2003)
262. Wildgoose G G et al. *Microchim. Acta* **152** 187 (2006)

263. Niessen R A H, de Jonge J, Notten P H L *J. Electrochem. Soc.* **153** A1484 (2006)
264. Rajalakshmi N et al. *Electrochim. Acta* **45** 4511 (2000)
265. Claye A S et al. *J. Electrochem. Soc.* **147** 2845 (2000)
266. Frackowiak E et al. *Carbon* **37** 61 (1999)
267. Wu G T et al. *J. Electrochem. Soc.* **146** 1696 (1999)
268. Goldsmith B R et al. *Science* **315** 77 (2007)
269. Larrimore L et al. *Nano Lett.* **6** 1329 (2006)
270. Rosenblatt S et al. *Nano Lett.* **2** 869 (2002)
271. Guan L et al. *Nano Lett.* **7** 1532 (2007)
272. Kissell K R et al. *J. Phys. Chem. B* **110** 17425 (2006)
273. Hatakeyama R, Li Y F *J. Appl. Phys.* **102** 034309 (2007)
274. Jeong G-H et al. *Chem. Commun.* 152 (2003)
275. Nishide D et al. *Chem. Phys. Lett.* **428** 356 (2006)
276. Botos Á et al. *Phys. Status Solidi B* **247** 2743 (2010)
277. Burteaux B et al. *Chem. Phys. Lett.* **310** 21 (1999)
278. Chamberlain T W et al. *ACS Nano* **4** 5203 (2010)
279. Hirahara K et al. *Phys. Rev. Lett.* **85** 5384 (2000)
280. Jeong G-H et al. *Carbon* **40** 2247 (2002)
281. Kataura H et al. *Synthet. Met.* **121** 1195 (2001)
282. Kataura H et al. *Appl. Phys. A* **74** 349 (2002)
283. Khlobystov A N et al. *J. Mater. Chem.* **14** 2852 (2004)
284. Khlobystov A N et al. *Angew. Chem. Int. Ed.* **43** 1386 (2004)
285. Khlobystov A N, Britz D A, Briggs G A D *Acc. Chem. Res.* **38** 901 (2005)
286. Luzzi D E, Smith B W *Carbon* **38** 1751 (2000)
287. Shimada T et al. *Physica E* **21** 1089 (2004)
288. Shiozawa H et al. *Phys. Rev. B* **73** 075406 (2006)
289. Simon F et al. *Chem. Phys. Lett.* **383** 362 (2004)
290. Sloan J et al. *Chem. Phys. Lett.* **316** 191 (2000)
291. Smith B W, Monthioux M, Luzzi D E *Chem. Phys. Lett.* **315** 31 (1999)
292. Smith B W, Luzzi D E *Chem. Phys. Lett.* **321** 169 (2000)
293. Yudasaka M et al. *Chem. Phys. Lett.* **380** 42 (2003)
294. Zhang Y et al. *Philos. Mag. Lett.* **79** 473 (1999)
295. Ashino M et al. *Nature Nanotechnol.* **3** 337 (2008)
296. Chiu P W et al. *Appl. Phys. Lett.* **79** 3845 (2001)
297. Gloter A et al. *Chem. Phys. Lett.* **390** 462 (2004)
298. Kitaura R et al. *Nano Lett.* **8** 693 (2008)
299. Okazaki T et al. *J. Am. Chem. Soc.* **123** 9673 (2001)
300. Okazaki T et al. *Physica B* **323** 97 (2002)
301. Pichler T et al. *Phys. Status Solidi B* **245** 2038 (2008)
302. Suenaga K et al. *Science* **290** 2280 (2000)
303. Débarre A et al. *Chem. Phys. Lett.* **380** 6 (2003)
304. Smith B W, Luzzi D E, Achiba Y *Chem. Phys. Lett.* **331** 137 (2000)
305. Suenaga K et al. *Phys. Rev. Lett.* **90** 055506 (2003)
306. Suenaga K et al. *Nano Lett.* **3** 1395 (2003)
307. Gimenez-Lopez M d C et al. *Chem. Commun.* **47** 2116 (2011)
308. Luzzi D E et al. *AIP Conf. Proc.* **591** 622 (2001)
309. Shiozawa H et al. *AIP Conf. Proc.* **786** 325 (2002)
310. Britz D A et al. *Chem. Commun.* 37 (2005)
311. Sun B-Y et al. *J. Am. Chem. Soc.* **127** 17972 (2005)
312. Chamberlain T W et al. *Chemistry A Eur. J.* **17** 668 (2011)
313. Chamberlain T W et al. *Nature Chem.* **3** 732 (2011)
314. Khlobystov A N *ACS Nano* **5** 9306 (2011)
315. Britz D A et al. *Chem. Commun.* 176 (2004)
316. Chamberlain T W et al. *J. Am. Chem. Soc.* **129** 8609 (2007)
317. Fan J et al. *Chem. Commun.* **47** 5696 (2011)
318. Briones A et al. *Phys. Status Solidi B* **248** 2488 (2011)
319. Guan L et al. *Carbon* **43** 2780 (2005)
320. Kocsis D et al. *Phys. Status Solidi B* **248** 2512 (2011)
321. Liu X et al. *Phys. Status Solidi B* **248** 2492 (2011)
322. Liu X et al. *Adv. Funct. Mater.* **22** 3202 (2012)
323. Plank W et al. *Phys. Status Solidi B* **246** 2724 (2009)
324. Sauer M et al. *Phys. Status Solidi B* **249** 2408 (2012)
325. Shiozawa H et al. *Phys. Status Solidi B* **244** 4102 (2007)
326. Shiozawa H et al. *Phys. Rev. B* **77** 153402 (2008)
327. Shiozawa H et al. *Phys. Status Solidi B* **245** 1983 (2008)
328. Shiozawa H et al. *Adv. Mater.* **20** 1443 (2008)
329. Shiozawa H et al. *Adv. Mater.* **22** 3685 (2010)
330. Li L-J et al. *Nature Mater.* **4** 481 (2005)
331. Shiozawa H et al. *Phys. Rev. Lett.* **102** 046804 (2009)
332. Shiozawa H et al. *Phys. Status Solidi B* **246** 2626 (2009)
333. Shiozawa H et al. *Phys. Status Solidi B* **247** 2730 (2010)
334. Loebick C Z et al. *J. Phys. Chem. C* **114** 11092 (2010)
335. Morgan D A, Sloan J, Green M L H *Chem. Commun.* 2442 (2002)
336. Kataura H et al. *AIP Conf. Proc.* **685** 349 (2003)
337. Tschirner N et al. *Phys. Status Solidi B* **247** 2734 (2010)
338. Yanagi K, Miyata Y, Kataura H *Adv. Mater.* **18** 437 (2006)
339. Takenobu T et al. *Nature Mater.* **2** 683 (2003)
340. Chancolon J et al. *J. Nanosci. Nanotech.* **6** 82 (2006)
341. Chernysheva M V et al. *Physica E* **40** 2283 (2008)
342. Wang Z, Shi Z, Gu Z *Carbon* **48** 443 (2010)
343. Kiang C-H et al. *J. Phys. Chem. B* **10**3 7449 (1999)
344. Borowiak-Palen E et al. *Chem. Phys. Lett.* **421** 129 (2006)
345. Borowiak-Palen E et al. *Phys. Status Solidi B* **243** 3277 (2006)
346. Govindaraj A et al. *Chem. Mater.* **12** 202 (2000)
347. Kharlamova M V, Niu J J *Appl. Phys. A* **109** 25 (2012)
348. Kharlamova M V, Niu J J *JETP* **115** 485 (2012) [*Zh. Eksp. Teor. Fiz.* **142** 547 (2012)]
349. Borowiak-Palen E et al. *Nanotechnology* **17** 2415 (2006)
350. Corio P et al. *Chem. Phys. Lett.* **383** 475 (2004)
351. Sloan J et al. *Chem. Commun.* 699 (1999)
352. Zhang Z L et al. *J. Mater. Res.* **15** 2658 (2000)
353. Kharlamova M V, Niu J J *JETP Lett.* **95** 314 (2012) [*Pis'ma Zh. Eksp. Teor. Fiz.* **95** 343 (2012)]
354. Chamberlain T W et al. *Chem. Sci.* **3** 1919 (2012)
355. Costa P M F J et al. *Chem. Mater.* **17** 6579 (2005)
356. Zoberbier T et al. *J. Am. Chem. Soc.* **134** 3073 (2012)
357. Kitaura R et al. *Angew. Chem. Int. Ed.* **48** 8298 (2009)
358. Nakanishi R et al. *Phys. Rev. B* **86** 115445 (2012)
359. Ayala P et al. *Phys. Rev. B* **83** 085407 (2011)
360. Zakalyukin R M et al. *Carbon* **46** 1574 (2008)
361. Eliseev A A et al. *Carbon* **48** 2708 (2010)
362. Eliseev A A et al. *Carbon* **50** 4021 (2012)
363. Flahaut E et al. *AIP Conf. Proc.* **59** 1283 (2001)
364. Sloan J et al. *Chem. Commun.* 1319 (2002)
365. Kharlamova M V *Appl. Phys. A* **111** 725 (2013)
366. Kharlamova M V et al. *Phys. Status Solidi B* **249** 2328 (2012)
367. Kharlamova M V et al. *J. Phys. Conf. Ser.* **345** 012034 (2012)
368. Kharlamova M V et al. *Eur. Phys. J. B* **85** 34 (2012)
369. Kharlamova M V et al. *Nanotechnol. Russ.* **4** 634 (2009) [*Ross. Nanotekhnol.* **4** (9 – 10) 77 (2009)]
370. Sloan J et al. *AIP Conf. Proc.* **591** 277 (2001)
371. Kitaura R et al. *Nano Res.* **1** 152 (2008)
372. Satishkumar B C, Taubert A, Luzzi D E *J. Nanosci. Nanotechnol.* **3** 159 (2003)
373. Xu C et al. *Chem. Commun.* 2427 (2000)
374. Brown G et al. *Chem. Commun.* 845 (2001)
375. Brown G et al. *Appl. Phys. A* **76** 457 (2003)
376. Kirkland A I et al. *Microsc. Microanal.* **11** 401 (2005)
377. Sloan J et al. *Inorg. Chim. Acta* **330** 1 (2002)
378. Sloan J et al. *C.R. Physique* **4** 1063 (2003)
379. Kharlamova M V et al. *JETP Lett.* **91** 196 (2010) [*Pis'ma Zh. Eksp. Teor. Fiz.* **91** 210 (2010)]
380. Bendall J S et al. *J. Phys. Chem. B* **110** 6569 (2006)
381. Chernysheva M V et al. *Physica E* **37** 62 (2007)
382. Hutchison J L et al. *J. Electron Microsc.* **53** 101 (2004)
383. Kiselev N A et al. *J. Microscopy* **232** 335 (2008)
384. Kiselev N A et al. *J. Microscopy* **246** 309 (2012)
385. Kumskov A S et al. *Carbon* **50** 4696 (2012)
386. Meyer R R et al. *Science* **289** 1324 (2000)
387. Sloan J et al. *Chem. Phys. Lett.* **329** 61 (2000)
388. Flahaut E et al. *Chem. Mater.* **18** 2059 (2006)
389. Philp E et al. *Nature Mater.* **2** 788 (2003)
390. Sloan J et al. *Angew. Chem. Int. Ed.* **41** 1156 (2002)
391. Friedrichs S, Falke U, Green M L H *ChemPhysChem* **6** 300 (2005)
392. Friedrichs S et al. *Microsc. Microanal.* **11** 421 (2005)
393. Sloan J et al. *J. Am. Chem. Soc.* **124** 2116 (2002)
394. Carter R et al. *Phys. Rev. Lett.* **96** 215501 (2006)
395. Sloan J et al. *Phys. Status Solidi B* **243** 3257 (2006)
396. Eliseev A A et al. *Chem. Mater.* **21** 5001 (2009)
397. Yashina L V et al. *J. Phys. Chem. C* **115** 3578 (2011)
398. Kumskov A S et al. *J. Microsc.* **248** 117 (2012)
399. Wang Z et al. *J. Am. Chem. Soc.* **132** 13840 (2010)
400. Li L-J et al. *Phys. Rev. B* **74** 245418 (2006)

401. Li L-J et al. *AIP Conf. Proc.* **893** 1047 (2007)
402. Hulman M et al. *Appl. Phys. Lett.* **85** 2068 (2004)
403. Friedrichs S et al. *Chem. Commun.* 929 (2001)
404. Friedrichs S et al. *Phys. Rev. B* **64** 045406 (2001)
405. Bajpai A et al. *Carbon* **50** 1706 (2012)
406. Thamavaranukup N et al. *Chem. Commun.* 1686 (2004)
407. Mittal J et al. *Chem. Phys. Lett.* **339** 311 (2001)
408. Kato T et al. *Appl. Phys. Lett.* **95** 083109 (2009)
409. Pagona G et al. *J. Am. Chem. Soc.* **130** 6062 (2008)
410. Kalbáč M et al. *J. Phys. Chem. B* **108** 6275 (2004)
411. Pichler T et al. *Phys. Rev. Lett.* **87** 267401 (2001)
412. Pichler T et al. *Phys. Rev. B* **67** 125416 (2003)
413. Eliseev A et al., in *Electronic Properties of Carbon Nanotubes* (Ed. J M Marulanda) (Rijeka, Croatia: InTech, 2011) p. 127
414. Eliseev A A et al. *Russ. Chem. Rev.* **78** 833 (2009) [*Usp. Khim.* **78** 901 (2009)]
415. Monthioux M *Carbon* **40** 1809 (2002)
416. Eletskii A V *Phys. Usp.* **43** 111 (2000) [*Usp. Fiz. Nauk* **170** 113 (2000)]
417. Eletskii A V *Phys. Usp.* **47** 1119 (2004) [*Usp. Fiz. Nauk* **174** 1191 (2004)]
418. Liu X et al. *Phys. Rev. B* **66** 045411 (2002)
419. Dresselhaus M S et al. *Carbon* **40** 2043 (2002)
420. Bandow S et al. *Phys. Rev. Lett.* **80** 3779 (1998)
421. Jorio A et al. *New J. Phys.* **5** 139 (2003)
422. Kuzmany H et al. *Eur. Phys. J. B* **22** 307 (2001)
423. Piscanec S et al. *Phys. Rev. B* **75** 035427 (2007)
424. Brown S D M et al. *Phys. Rev. B* **61** R5137 (2000)
425. Kalbac M et al. *Nano Lett.* **8** 1257 (2008)
426. Bachilo S M et al. *Science* **298** 2361 (2002)
427. Bachilo S M et al. *J. Am. Chem. Soc.* **125** 11186 (2003)
428. O'Connell M J et al. *Science* **297** 593 (2002)
429. Kramberger C et al. *Phys. Rev. B* **75** 235437 (2007)
430. Batson P E *Phys. Rev. B* **48** 2608 (1993)
431. Kramberger C, Pichler T, in *Advances in Carbon Nanomaterials: Science and Applications* (Ed. N Tagmatarchis) (Singapore: Pan Stanford Publ., 2012) p. 131
432. Liu X et al. *Phys. Rev. B* **65** 045419 (2002)
433. Dresselhaus M S, Jorio A, Saito R *Annu. Rev. Condens. Matter Phys.* **1** 89 (2010)
434. Ayala P et al. *Phys. Rev. B* **80** 205427 (2009)
435. Ishii H et al. *Nature* **426** 540 (2003)
436. Gal'pern E G et al. *Chem. Phys. Lett.* **214** 345 (1993)
437. Du M-H, Cheng H-P *Phys. Rev. B* **68** 113402 (2003)
438. Dubay O, Kresse G *Phys. Rev. B* **70** 165424 (2004)
439. Lu J et al. *Phys. Rev. B* **68** 121402(R) (2003)
440. Okada S, Otani M, Oshiyama A *Phys. Rev. B* **67** 205411 (2003)
441. Otani M, Okada S, Oshiyama A *Phys. Rev. B* **68** 125424 (2003)
442. Rochefort A *Phys. Rev. B* **67** 115401 (2003)
443. Lu J et al. *Phys. Rev. Lett.* **93** 116804 (2004)
444. García-Suárez V M, Ferrer J, Lambert C J *Phys. Rev. Lett.* **96** 106804 (2006)
445. Sceats E L, Green J C *J. Chem. Phys.* **125** 154704 (2006)
446. Ivanovskaya V V, Köhler C, Seifert G *Phys. Rev. B* **75** 075410 (2007)
447. Xie Y, Zhang J M, Huo Y P *Eur. Phys. J. B* **81** 459 (2011)
448. Kang Y-J et al. *Phys. Rev. B* **71** 115441 (2005)
449. Sun Y, Yang X, Ni J *Phys. Rev. B* **76** 035407 (2007)
450. Meunier V et al. *Nano Lett.* **9** 1487 (2009)
451. Zhou J et al. *J. Phys. Chem. C* **114** 15347 (2010)
452. Parq J-H, Yu J, Kim G *J. Chem. Phys.* **132** 054701 (2010)
453. Du X-J et al. *Eur. Phys. J. B* **72** 119 (2009)
454. Fagan S B et al. *Chem. Phys. Lett.* **406** 54 (2005)
455. Li W et al. *Phys. Rev. B* **74** 195421 (2006)
456. Sceats E L, Green J C, Reich S *Phys. Rev. B* **73** 125441 (2006)
457. Chiu P W et al. *Appl. Phys. A* **76** 463 (2003)
458. Hornbaker D J et al. *Science* **295** 828 (2002)
459. Kato T, Hatakeyama R, Tohji K *Nanotechnology* **17** 2223 (2006)
460. Lee J et al. *Nature* **415** 1005 (2002)
461. Li Y F et al. *Appl. Phys. Lett.* **90** 173127 (2007)
462. Obergfell D et al. *Phys. Status Solidi B* **243** 3430 (2006)
463. Okazaki T et al. *Appl. Phys. A* **76** 475 (2003)
464. Service R F *Science* **292** 45 (2001)
465. Shimada T et al. *Appl. Phys. Lett.* **81** 4067 (2002)
466. Zhao J, Xie R *J. Nanosci. Nanotechnol.* **3** 459 (2003)
467. Lota G et al. *Chem. Phys. Lett.* **434** 73 (2007)
468. Zhukov A A et al. *JETP* **109** 307 (2009) [*Zh. Eksp. Teor. Fiz.* **136** 362 (2009)]
469. Benjamin S C et al. *J. Phys. Condens. Matter* **18** S867 (2006)